PHOTO-ASSISTED ELECTRO[redacted]ALYSIS OF WATER USING p-TYPE III-V SEMICONDUCTORS

GARY ROBERT HANCOCK

PHOTO-ASSISTED ELECTROLYSIS OF WATER USING p-TYPE III-V SEMICONDUCTORS

by

© Gary Robert Hancock, B.Sc. (Hons.)

Submitted in partial fulfillment of
the requirements for the degree of
Master of Science

Department of Chemistry
Memorial University of Newfoundland
St. John's, Newfoundland
Canada A1B 3X7

March, 1984

ABSTRACT

The recent interest in photoelectrochemical methods of solar energy conversion has led to the investigation of many semiconductors for their suitability as electrodes for the process. Attempts have also been made to improve the photoelectrochemical performance of many of these semiconductor electrodes by various surface treatments.

In the first part of this work, the current density-potential characteristics for the photo-assisted electrolysis of water were compared for p-GaP, p-GaAs and p-InP photocathodes, unplated and with thin electrodeposits (2-200 monolayers) of platinum or palladium. The photocathodes were used in a cell with a platinum anode and 0.5 M H_2SO_4 as electrolyte. For all three semiconductors the noble metal platings resulted in favourable positive potential shifts of the cathodic current-potential curves. Positive energy conversion efficiencies were realized (maximum value of 0.03% in 200 mW.cm^{-2} simulated sunlight) for GaP only. It is suggested that the noble metal atoms plated on the surface improve performance by catalytic acceleration of the hydrogen evolution reaction (h.e.r.).

In the second part of this work photoelectrochemical kinetic parameters were determined for the h.e.r. on the same three semiconductors in 0.5 M H_2SO_4. Room temperature measurements showed the results to conform reasonably well to equations derived by W.L. Ahlgren, based largely on theory developed by J.F. Dewald and H. Gerischer, and modified here for the particular situation of interest. The method involved recording current-potential characteristics at several light intensities and extracting data from them to construct a so-called Ahlgren plot to yield the exchange current density. A jacketed cell was employed later to enable exchange current densities at several temperatures to be determined and used to construct Arrhenius plots. The average values of the exchange current densities (in $\mu A.cm^{-2}$ at 298 K) were 5×10^{-2}, 3×10^{-2} and 2×10^{-4} for GaP, GaAs and InP, respectively. The weighted mean activation enthalpies, in $kJ.mol^{-1}$, were 16.0 for GaP, 25.7 for GaAs, and 61.6 for InP. These results suggest that for the h.e.r. on the bare (unplated) electrodes, GaP is a more suitable electrode than GaAs, and both are much better than InP.

The agreement with theory and problems of achieving reproducibility are discussed. The significance of the exchange current densities and activation enthalpies determined by this method is explained and a comparison of the exchange current densities with those for the h.e.r. on some metals is presented. Some recent promising work by other researchers is documented and suggestions for future experiments made.

ACKNOWLEDGEMENTS

I first of all wish to express my gratitude to my supervisor, Dr. Frank R. Smith, for initiating my interest in photoelectrochemistry and for his encouragement and assistance during the course of the work.

I am indebted to the staff of Memorial University's Technical Services Department for their technical assistance with apparatus and equipment. I would like to single out Mr. George Pardy and Mr. Keith Decker of the electronics shop and glassblowers Mr. Doug Seymour, Mr. Martin Hattswell and Mr. Tom Perks for particular recognition.

Helpful advice and assistance from Dr. R.G. Barlatt, an associate during the earlier part of the work, were also greatly appreciated.

I also wish to thank Miss Teresa Barker for typing this thesis and Mrs. Cathy Chen and Mr. John Kane who between them prepared the figures.

Finally, the financial support of the Natural Sciences and Engineering Research Council, in the form of a Postgraduate Scholarship, is gratefully acknowledged.

TABLE OF CONTENTS

Page

ABSTRACT ii

ACKNOWLEDGEMENTS iv

LIST OF TABLES vii

LIST OF FIGURES viii

LIST OF SYMBOLS xii

I. INTRODUCTION 1

II. THEORY 4

Introduction 4

The semiconductor-electrolyte junction: dark and illuminated 4

The energy balance and overall energy conversion efficiency 9

The mechanism of the hydrogen evolution reaction (h.e.r.) on illuminated p-type III-V semiconductors 11

The current-potential relations of photoelectrolytic cells 13

III. EXPERIMENTAL 31

Photoelectrochemical Cells 31

Semiconductor Electrodes - Preparation and Mounting 33

Instrumentation 40

Materials 43

Reference and Counter Electrodes 45

Cleaning 45

Methods 47

IV. RESULTS 56

1. Preliminary Studies and Noble Metal Plating Experiments 56

a. Gallium phosphide 56

page

b. Gallium arsenide 59

c. Indium phosphide 61

2. Photoelectrochemical Kinetics Measurements 64

i. Preliminary work 64

a. Gallium phosphide 64

b. Gallium arsenide 69

c. Indium phosphide 69

d. Summary 69

ii. Variable temperature experiments 77

a. Gallium phosphide 77

b. Gallium arsenide 84

c. Indium phosphide 86

V. DISCUSSION 101

1. Noble Metal-Plating Experiments 101

2. Photoelectrochemical Kinetics 105

i. Agreement of results with theory 105

ii. Difficulties encountered 106

iii. The significance of the exchange currents and enthalpies of activation determined here 107

iv. Exchange currents 109

v. Activation enthalpies 112

vi. Summary-future research 112

REFERENCES 114

APPENDIX 117

LIST OF TABLES

Page

Table 1. Some properties of the semiconductor materials used . . 36

Table 2. A summary of the results of the preliminary photoelectrochemical kinetics experiments with GaP, GaAs and InP 65

Table 3. Exchange current densities as a function of temperature for hydrogen evolution on illuminated p-GaP (two experiments) 82

Table 4. The values of $\Delta H^{\ddagger}$ and $\ln(A^{\ddagger})$ obtained from weighted least squares analysis of the Arrhenius plots for hydrogen evolution on illuminated p-GaP 85

Table 5. Exchange current densities as a function of temperature for hydrogen evolution at an illuminated p-GaAs electrode 90

Table 6. The values of $\Delta H^{\ddagger}$ and $\ln(A^{\ddagger})$ obtained from weighted least squares analysis of the Arrhenius plots for hydrogen evolution on illuminated p-GaAs 90

Table 7. Some results of early variable temperature experiments for hydrogen evolution on illuminated p-InP 93

Table 8. A summary of the results of one of the later variable temperature experiments with p-InP 99

Table 9. A summary of the values of $\Delta H^{\ddagger}$ and $\ln(A^{\ddagger})$ for hydrogen evolution obtained from the weighted least squares analysis of Arrhenius plots of three different experiments using p-InP 99

Table 10. Exchange current densities on some metals and on the illuminated semiconductor electrodes studied here for the hydrogen evolution reaction at 298 K 113

Table 11. Comparison of the activation enthalpies and pre-exponential factors determined for the hydrogen evolution reaction on the three semiconductors studied in this work 113

LIST OF FIGURES

Page

Figure 1. Positions of the energy bands and the Fermi levels for the semiconductor-electrolyte-metal system under various conditions 5

Figure 2. Carrier concentrations and band bendings for a p-type semiconductor with accumulation, inversion and depletion layers, and under flat band conditions 7

Figure 3. The band gap energies and the approximate positions of the conduction and valence band edges in 0.5 M H_2SO_4 for the three semiconductors studied in this work 25

Figure 4. The illuminated p-type semiconductor-electrolyte interface at the potential of zero current and with current flowing 27

Figure 5. Two diagrams of a typical cell used for room temperature photoelectrochemical measurements 32

Figure 6a. The jacketed photoelectrochemical cell, showing the quartz optical flat at the front 34

Figure 6b. The jacketed photoelectrochemical cell equipped with, front, a semiconductor electrode, to its right, a palladium reference electrode, and behind, a platinum counter electrode 35

Figure 7. Current-voltage characteristic for two In/Zn alloy contacts on GaP 38

Figure 8. The two types of glass electrode holders used in this work - (a) horizontal and (b) vertical - and (c) the mounting arrangement for semiconductor electrode specimens on the holders 39

Figure 9. A schematic diagram showing the arrangement of the lamp, other optical equipment, and the cell, along the optical rail 41

Figure 10. A schematic diagram of the gas handling system for supplying very pure argon to the photoelectrochemical cells 44

Figure 11. Diagrams showing the construction of typical reference and counter electrodes used in this work. . 46

Page

Figure 12. The effect of the potential scan rate on the current-potential characteristic for hydrogen evolution on illuminated p-GaP in 0.5 M H_2SO_4 52

Figure 13. The effect of total time in solution on the current-potential characteristic for hydrogen evolution on illuminated p-GaP in 0.5 M H_2SO_4 . . . 53

Figure 14. Representative current-potential curves for hydrogen evolution on illuminated p-GaAs and p-GaP 57

Figure 15. The effect of plating 40 atoms.$\AA^{-2}$ of palladium on the current-potential characteristic for hydrogen evolution on illuminated p-GaP in 0.5 M H_2SO_4 58

Figure 16. Current stability (time dependence of current at constant potential) for hydrogen evolution on illuminated p-GaP plated with various amounts of palladium 60

Figure 17. Best shift of current-potential characteristic for hydrogen evolution on illuminated p-GaAs in 0.5 M H_2SO_4, obtained by plating 0.4 atoms.$\AA^{-2}$ of platinum 62

Figure 18. The effect of light intensity on the current-potential characteristics for hydrogen evolution on p-GaP 66

Figure 19. Typical current vs. light intensity plots at several values of the overpotential for hydrogen evolution on p-GaP in 0.5 M H_2SO_4 67

Figure 20. An Ahlgren plot for hydrogen evolution on illuminated p-GaP in 0.5 M H_2SO_4; T = 297 ± 1 K . . . 68

Figure 21. The effect of light intensity on the current-potential characteristic for hydrogen evolution on p-GaAs 70

Figure 22. Typical current vs. light intensity plots at several overpotentials for hydrogen evolution on p-GaAs in 0.5 M H_2SO_4 71

Figure 23. Ahlgren plot for hydrogen evolution on illuminated p-GaAs in 0.5 M H_2SO_4; T = 297 ± 1 K 72

page

Figure 24. Current-potential characteristics at several light intensities for hydrogen evolution on p-InP in 0.5 M H_2SO_4 . . . 74

Figure 25. Typical current vs. light intensity plots at several overpotentials for hydrogen evolution on p-InP in 0.5 M H_2SO_4 . . . 75

Figure 26. Ahlgren plot for hydrogen evolution on illuminated p-InP in 0.5 M H_2SO_4 . . . 76

Figure 27. The effect of temperature on the current-potential characteristics for hydrogen evolution on illuminated p-GaP . . . 78

Figure 28. Representative current density vs. light intensity plots at several overpotentials for hydrogen evolution on p-GaP. T = 306.8 K . . . 79

Figure 29. Typical Ahlgren plots at several temperatures for hydrogen evolution on illuminated p-GaP . . . 81

Figure 30. The Arrhenius plots for hydrogen evolution on illuminated p-GaP from the data summarized in Table 3 . . . 83

Figure 31. The temperature dependence of the current-potential curves for hydrogen evolution on illuminated p-GaAs . 87

Figure 32. Typical current density vs. light intensity plots at several overpotentials for hydrogen evolution on p-GaAs. T = 306.9 K . . . 88

Figure 33. Representative Ahlgren plots at three temperatures for hydrogen evolution on illuminated p-GaAs . . . 89

Figure 34. Arrhenius plots for hydrogen evolution on illuminated p-GaAs (data from two experiments using different electrodes) . . . 91

Figure 35. Current-potential curves at various temperatures for hydrogen evolution on illuminated p-InP . . . 95

Figure 36. Typical current vs. light intensity plots at several overpotentials for hydrogen evolution on p-InP . . . 96

Figure 37. Typical Ahlgren plots at several temperatures for hydrogen evolution on illuminated p-InP in 0.5 M H_2SO_4 . . . 98

page

Figure 38. Arrhenius plots for hydrogen evolution on illuminated p-InP (data from two experiments using different electrodes) 100

Figure 39. Hypothetical energy level diagrams for the spontaneous photoelectrolysis of water with two semiconductor electrodes - a p-type cathode and an n-type anode 104

Figure 40. Hypothetical Ahlgren plots showing the effect of the relative magnitude of the light intensities used upon the values of the exchange current density obtained when Ahlgren's convention and that adhered to in this thesis for $\eta = 0$ are followed 111

LIST OF SYMBOLS

$\bar{a}$	average light absorption coefficient
a(E)	light absorption coefficient
$A^{\ddagger}$	Arrhenius pre-exponential factor
b	pertaining to the semiconductor or electrolyte bulk (subscript)
c	pertaining to the semiconductor conduction band (subscript)
[illegible]	concentration
D_n	diffusion coefficient for electrons
e^-	electron
E	energy
E_B	bias voltage
E_F	Fermi-level
[illegible]	flat-band potential
E_g	semiconductor band gap energy
E_i	potential at which the potential drop across the semiconductor-electrolyte interface is $V_H + V_B$
E_o	threshold energy of light for electron-hole pair creation
E^o	potential of zero current
F	Faraday's constant
g(x)	electron generation rate due to light absorption at a depth x into the semiconductor
ΔG	free energy change
h	Planck's constant
h^+	hole
h.e.r.	hydrogen evolution reaction
$\Delta H^{\ddagger}$	enthalpy of activation
ΔH_f^o	standard enthalpy of formation

i	current density
i_+	anodic current density
i_-	cathodic current density
i_c	current density due to charge transfer with the conduction band
i_{co}	conduction band exchange current density
i_d	current density in the dark
i_o	exchange current density
i_s	saturation value of the dark current density
i_v	current density due to charge transfer with the valence band
i_{vo}	valence band exchange current density
iR	resistive loss in the electrolyte
I	light intensity
J_n	diffusive electron flux
$\vec{J}_n$	electron flux entering the depletion layer from the bulk
k_+	rate constant of anodic half-reaction
k_-	rate constant of cathodic half-reaction
L_n	diffusion length for electrons
n	number of electrons involved in an electrochemical reaction
n_o	electron concentration in the semiconductor bulk
n_s	electron concentration at the surface
n_s^o	surface electron concentration at equilibrium
n_w	electron concentration at the inside edge of the depletion layer
p_s	hole concentration at the surface
p_s^o	surface hole concentration at equilibrium

R	gas constant
$R(E)$	surface reflectance
s	pertaining to the interfacial region (subscript)
SC	semiconductor
t	time
T	temperature
v	pertaining to the semiconductor valence band (subscript)
V	potential drop across the interface with current flowing
V^o	potential drop across the interface at the potential of zero current
V_B	band bending with current flowing
V_B^o	band bending at the potential of zero current
V_H	potential drop in the Helmholtz layer with current flowing
V_H^o	potential drop in the Helmholtz layer at the potential of zero current
w	width of the semiconductor depletion layer
$W(E,x)$	intensity of light of energy E at position x
$W_o(E)$	spectral radiation intensity at the semiconductor surface
x	distance into the semiconductor from the surface
$\vec{\alpha}$	transfer coefficient (arrow indicating the cathodic direction of electron movement)
α/β PdH	abbreviation for the palladium hydride reference electrode
γ	conversion factor from light to electrical energy
Δ	$\eta F/RT$
η	overpotential
η_a	anodic overpotential
η_c	cathodic overpotential
η_H	overpotential occurring in the Helmholtz layer

η_{sc}	overpotential occurring in the semiconductor space charge region
ν	frequency of light
ν_s	surface electron-hole recombination velocity
ξ	percentage energy conversion efficiency
ρ	fraction of the overpotential occurring in the Helmholtz layer of the electrolyte
τ_n	average electron lifetime in the semiconductor
ϕ	quantum yield
ϕ_o	potential drop in the Helmholtz layer with current flowing
ϕ_o^o	potential drop in the Helmholtz layer at equilibrium
ϕ_s	saturation value of the quantum yield

I. INTRODUCTION

Because the bandgap energies of many semiconductors lie within the range of energies of the solar spectrum, semiconductors absorb solar radiation, promoting valence band electrons to the conduction band and leaving holes in the valence band. Under suitable conditions of band bending at the semiconductor surface, the charge carriers can be separated so that they may effect useful processes, such as electricity generation (photovoltaic cells) or the production of useful fuels or other chemicals (photoelectrolytic and photoelectrosynthetic cells).

Only within the last ten years or so have these possibilities been realized and the use of semiconductor electrodes to convert solar energy into more practical energy forms become of widespread interest. This thesis is concerned with the photo-assisted (i.e. energy additional to solar energy is required) electrolysis of water to hydrogen and oxygen. This process has been the focus of a great deal of research since the pioneering work of Fujishima and Honda (1), who demonstrated the successful photoelectrolysis of water using a titanium dioxide anode, a platinum cathode and ultraviolet light. Since then, a large volume of work, using a wide range of semiconductor materials, various electrolytes, and particular surface treatments, in attempts to improve the photoelectrolytic performance, has been published. Reviews of this early work have been written by Harris and Wilson (2), Nozik (3), and Tomkiewicz and Fay (4). Some recent progress, with emphasis on promising configurations, has been discussed by Parkinson (5).

The present work has focussed on the use of the p-type III-V semiconductors GaP, GaAs and InP as photocathodes in the photo-assisted electrolysis of water. Memming and Schwandt (6) seem to have been the first to observe hydrogen evolution on illuminated p-GaP at potentials positive of the equilibrium potential of the H_3O^+/H_2 couple. Of the three compounds studied in this research, GaP has been the subject of the greatest volume of work, some of the more relevant (to this work) of which have been cited in references ((7) - (15)). In earlier research on GaAs and InP, the consensus was that the additional bias voltages (the aforementioned additional energy input) required were so large that efficient conversion of solar energy to hydrogen was improbable (8, 16).

Investigations by Nakato et al. (17) had shown that thin electrodeposits of metals such as platinum and palladium on p-GaP resulted in favourable shifts of the current-potential relationships for hydrogen evolution. The purpose of a part of the present work was to repeat the studies of Nakato et al. and to extend the range of thickness of the noble metal films to larger values, in order to optimize the effect, and to expand the investigation to include GaAs and InP, with the anticipation that the current-potential relationships on these materials could be sufficiently shifted to substantially reduce the required bias voltage.

In the second part of this work, an attempt has been made to measure hydrogen evolution reaction (h.e.r.) rates on these semiconductors by a novel method. It has been suggested (18, 19) that kinetics, rather than thermodynamics, is the limiting factor in the h.e.r. Experiments were performed in which the current was measured as a function of potential and light intensity and the results analyzed using a method modified from one developed by Ahlgren (20, 21). The reaction rates determined were expressible as exchange current densities. From the temperature dependence of these rates, activation enthalpies and Arrhenius pre-exponential factors have been derived for the h.e.r. occurring at the three p-type semiconductors, GaP, GaAs and InP.

II. THEORY

Introduction

The two main properties which distinguish a semiconductor from a metal, the lower conductivity and the existence of the so-called "forbidden band", of width equal to the bandgap, lead to important differences in the properties of semiconductor-electrolyte interfaces as compared with the metal-electrolyte interface.

As noted by Dewald (22), the low, readily-variable electron density permits extension of electrical fields deep into the semiconductor. Also, two types of charge carriers, conduction band electrons and valence band holes, are distinguishable because of the forbidden energy gap, within which no charge carriers are permissible.

It should be added that since the bandgap energy is usually of the order of magnitude of energies present in the solar spectrum, illumination with sunlight can drastically alter the surface properties by promoting valence band electrons to the conduction band, thus creating electron-hole pairs which, if separated, can act to effect redox reactions with a suitable electrolyte.

The semiconductor-electrolyte junction - dark and illuminated

Many excellent reviews concerning the semiconductor-electrolyte junction and how it is affected by light are now available. Those of Harris and Wilson (2), Nozik (3), and Tomkiewicz and Fay (4) have proved particularly helpful in the development of this section.

When a semiconductor is brought into contact with an electrolyte, there will in general be a difference in the average energy, or Fermi level, E_F, of electrons in the two phases (see Figure 1). By conven-

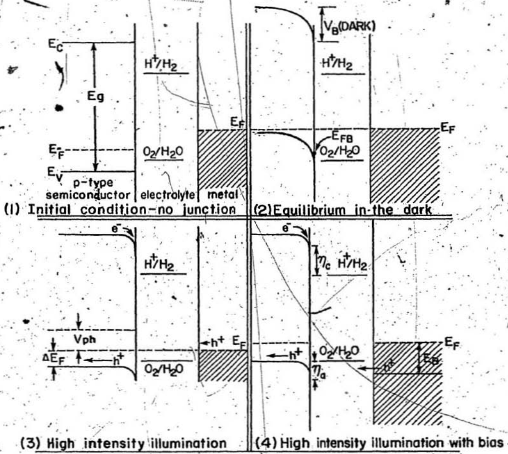

(1) Initial condition–no junction

(2) Equilibrium in the dark

(3) High intensity illumination

(4) High intensity illumination with bias

Figure 1. Energy level diagrams for the p-type semiconductor-electrolyte-metal electrode system under the indicated conditions (from Nozik's diagram (3), modified for a p-type semiconductor). Symbols: E_c, E_v - conduction and valence band edges respectively; E_F - Fermi level; V_B - band bending; V_{ph} - photovoltage; ΔE_F - difference between Fermi level and valence band edge; E_B - bias voltage; η_c, η_a - anodic and cathodic Helmholtz layer potential drops; E_{FB} - flat-band potential; E_g - band gap energy.

tion, E_F for a semiconductor is equal to the electronic work function of the semiconductor measured with respect to the electron vacuum level and for extrinsic semiconductors is usually near the band edge of the band containing excess charge carriers. The nature and concentration of the redox species present in solution determines E_F for the electrolyte, measured with respect to a suitable reference electrode, often the standard hydrogen electrode (SHE). As Figure 1 shows, the two energy scales are directly related.

Because the Fermi levels are initially different, charge transfer across the interface occurs and the semiconductor bands bend to bring the Fermi levels to equality. Depending on the initial positions of the Fermi levels, this charge transfer can result in accumulation, inversion, or depletion layers in the semiconductor space charge region (see Figure 2). An accumulation or inversion layer is formed when a relatively large increase in the majority or minority carrier concentration, respectively, occurs in the space charge region. A depletion layer forms when the space charge region is deficient in majority carriers. Since the minority carrier concentration is already low, the region is truly "depleted" of charge and becomes essentially insulating (see Figure 2). A depleted semiconductor surface is of interest in photoelectrolysis since it permits light-generated minority carriers to reach the surface, giving a large photo-effect since the concentration of these carriers is initially low and more sensitive to illumination than the concentration of the majority carriers, which is initially much larger. The bending of the bands, measured with respect to the flatband potential, E_{FB}, the potential at which the bands are flat right out

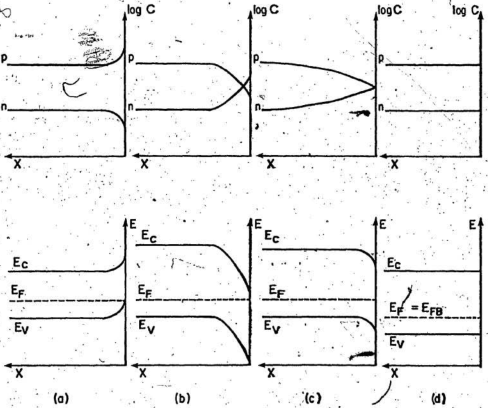

Figure 2. Carrier concentration (c) and band bending for a p-type semiconductor with: (a) accumulation layer, (b) inversion layer, (c) depletion layer and (d) flat bands. Based on Gerischer's diagram (23a) for n-type semiconductors. E_c and E_v are the conduction and valence band edge energies respectively, p and n represent holes and electrons and X is the distance into the semiconductor.

to the surface (see Figures 1 and 2), presents an obstacle to further charge transfer as the Fermi levels become equal.

If the surface-depleted semiconductor is illuminated with light with photon energy greater than the bandgap energy, the equilibrium is again disturbed by generation of electron-hole pairs. The increased populations of electrons in the conduction band and of holes in the valence band result in the Fermi level of the semiconductor being driven back towards E_{FB} (Figure 1). Thus E_{FB} sets a limit on the minority carrier energy at the surface and hence on which redox reactions are spontaneous at the semiconductor-electrolyte interface. Illumination evidently decreases the band bending. In suitable cases, sufficient band bending remains to effect a separation of electron-hole pairs, minority carriers migrating to the surface and majority carriers moving towards the bulk. If redox species of suitable energy are present in the electrolyte, then redox reactions can occur.

For a p-type semiconductor, photo-excited minority carrier electrons may effect reduction at the semiconductor-electrolyte interface while holes, after being transported via an external contact to a suitable counter-electrode, effect oxidation (see Figure 1). Actually an electron from a donor species in solution migrates in the latter case, but the effect is the same as if one imagines hole migration.

If the redox reactions driven at the two electrodes are each the reverse of the other, electricity is generated and there is no net change in the electrolyte composition. Such a device is an electrochemical photovoltaic cell. If the redox reactions are different, photoelectrolysis occurs and there is consequent depletion of certain species in the electrolyte. An example of this is the photoelectrolysis of water to produce hydrogen and oxygen in what Nozik (9) has labelled a Schottky-type cell, i.e. a cell with one semiconductor and one metallic electrode, which is the process of interest in this thesis.

In many cases, simply illuminating the semiconductor does not suffice to effect the desired reactions. The position of the semiconductor bands may not be optimal with respect to the energies of the redox species involved in the electrolysis and some additional electrical energy, in the form of a bias voltage, may be required to drive the overall reaction. Even if the band-positions are adequate the reactions may be too slow (i.e. kinetically hindered), in the absence of a bias voltage, to be feasible for solar energy conversion. When bias voltages are required, the phenomenon is called photo-assisted electrolysis and is also depicted in Figure 1.

Bias voltages were required for appreciable electrolysis currents with all of the semiconductors studied in this thesis. The bias voltage must be taken into account when the overall energy conversion efficiency for photoelectrolysis is calculated. If the bias voltage is not too large, positive energy conversion efficiencies may still be realized.

The energy balance and overall energy conversion efficiency

The energy balance for photo-assisted electrolysis can be written, with reference to Figure 1, following (3),

$$E_g + E_B - V_B - \Delta E_F = \frac{\Delta G}{nF} + \eta_a + \eta_c + iR \qquad [1]$$

where E_g is the semiconductor bandgap energy, E_B the applied bias voltage, V_B the band bending, ΔE_F the difference between the Fermi level and the top of the valence band, ΔG is the free energy of electrolysis for the reaction involving n electrons, F is Faraday's constant, η_a and η_b are the anodic and cathodic overpotentials, respectively, and iR is the resistive loss in the electrolyte. To appreciate equation [1], follow the paths of an electron-hole pair generated near the semiconductor surface, remembering that the bands are drawn for electron energies so that a higher position means a lower energy for holes. In employing [1], one must also ensure that the units are compatible since some quantities, such as E_g, are usually expressed in molecular units, i.e. eV, while others, like ΔG, are usually given in molar units. These conversions are uncomplicated since, by definition, 1 eV for a molecule is equivalent to 1F x 1V for a mole.

The overall percentage/energy conversion efficiency for the photoelectrolysis of water has been given by Tomkiewicz and Woodall (8a), as

$$\xi = \frac{(1.48 - E_B)i}{I} \times 100 \qquad [2]$$

In [2], i is the current density of hydrogen evolution, I is the incident light intensity, E_B is as defined above, and the constant, 1.48 V, is $\Delta H_f^o/2F$ for water at 298 K. Equation [2] gives the maximum possible efficiency as it assumes that the hydrogen produced can be collected and burned with 100 per cent efficiency.

The mechanism of the hydrogen evolution reaction (h.e.r.) on illuminated p-type III-V semiconductors

The steps of the h.e.r. mechanism at an illuminated p-type semiconductor are listed below, after (12, 15, 24).

$SC + h\nu \longrightarrow h^+_{vb} + e^-_{cb} + SC$ [3] (photogeneration)

$e^-_{cb} \longrightarrow e^-_{cs}$ [4a] (diffusion)

$h^+_{vb} \longrightarrow h^+_{vs}$ [4b] (diffusion)

$H_3O^+_b \longrightarrow H_3O^+_s$ [5] (mass transport)

$SC + e^-_{cs} + H_3O^+_s \longrightarrow SC\text{-}H + H_2O$ [6] (charge transfer)

$SC\text{-}H + H\text{-}SC \longrightarrow H_2 + 2SC$ [7a] (H atom recombination)

$SC\text{-}H + H_3O^+_s + e^-_{cs} \longrightarrow H_2 + H_2O + SC$ [7b] (electrochemical desorption)

$h^+_{vs} + SC\text{-}H + H_2O \longrightarrow H_3O^+_s + SC$ [8] (oxidation)

In [3] - [8], e^- is an electron, h^+ represents a hole and the subscripts c, v, s and b are abbreviations for conduction band, valence band, surface, and bulk, respectively. The semiconductor electrode is represented by SC, while SC-H means a hydrogen atom adsorbed on the semiconductor surface.

Thus, the photogenerated minority carrier, e^-_{cb}, after diffusing to the surface can participate in step [6], charge transfer with hydronium ions, $H_3O^+_s$, which have migrated from the electrolyte bulk to the semiconductor-electrolyte interface. The adsorbed hydrogen atoms, SC-H, thereby formed, can then react to produce H_2 by a purely chemical [7a] or by an electrochemical [7b] process. Step [8] allows for the possibility of reoxidation of adsorbed hydrogen atoms by holes. Electron-hole recombination via surface states involves steps [6] and

[8] together. Such recombination may also occur directly or via surface trap mechanisms.

Certain noble metals, such as platinum and palladium, are known to catalyze the h.e.r. (25), probably by providing sites to facilitate the desorption steps, [7a] and [7b]. This was the motivation for attempting to improve the current-potential characteristics of the photo-assisted electrolysis by electrodepositing thin films of such metals on the semiconductors.

The rate of the desired overall reaction, $2H_3O^+_{(aq)} + 2h\nu \rightarrow H_2 + 2H_2O$, at the semiconductor cathode, is that of the rate-determining step in the above sequence. For metals, steps analogous to [6], [7a] or [7b] are rate-limiting, in the absence of mass transport control in the solution phase, as electron supply is unlikely to limit the rate. For semiconductors, however, with inherently low charge carrier concentrations and losses by recombination, the rate at which minority carriers arrive at the interface may be the limiting step. The observation that the photocurrents of photoelectrolysis cells are light intensity-dependent (20,21,26) in a suitable potential range lends support to this idea.

With either polychromatic or monochromatic illumination, the quantum yield (ϕ), the ratio of the number of atoms of hydrogen produced to the incident light quanta, is usually much less than 1 (11), in the usual range of potentials. Thus, step [3] generally produces electrons at a greater rate than they are consumed by subsequent charge transfers. Step [3] can still influence the rate because it affects the concentration of electrons involved in subsequent rate determining steps. Only if ϕ approaches unity, i.e. transport of carriers becomes very efficient, could step [3] limit the rate.

Mass transport hindrance can be minimized by efficient stirring of the electrolyte. Charge transfer, exemplified by [6] or by the combination of [6] and [7b], can only be satisfactorily studied if theoretical current-potential expressions encompassing the roles of the light intensity and carrier migration in the semiconductor have been developed. This is the purpose of the next section.

The current-potential relations of photoelectrolytic cells

The development of theoretical expressions for the current-potential relation of an electrochemical reaction at a semiconductor-electrolyte interface follows closely that for the analogous situation at a metal-electrolyte interface (see, for example, Myamlin and Pleskov (27)). For the general redox reaction

$$A^{n+} + e^- \rightleftharpoons A^{(n-1)+} \qquad [9]$$

the overall current density is written

$$i = i_+ + i_- \qquad [10]$$

where i_+ and i_- denote the anodic and cathodic contributions, respectively, to the total current density i. The convention that anodic current is positive, and cathodic current negative, will be followed.

The cathodic current is proportional to the concentration of the species A^{n+}, designated $C_A n+$, to the number of electrons at the interface, n_s, and to the probability of electron transfer to the ion, i.e.

$$i_- = k_-(C_A n+) n_s \exp\left(\frac{-\vec{\alpha} F \phi_{\alpha}}{RT}\right) \qquad [11]$$

In [11] k_- is the rate constant, $\overrightarrow{\alpha}$ is the transfer coefficient with the arrow indicating the cathodic direction of electron flow, and ϕ_o is the potential drop in the Helmholtz layer of the electrolyte (the matter of potential distribution in the interfacial region will be addressed later).

The presence of the term n_s distinguishes [11] from the corresponding relation for metals, since for the latter n_s is large and current-independent and is generally subsumed in k_-.

The corresponding expression to [11] for i_+ is

$$i_+ = k_+ (C_A (n-1)+) \exp\left(\frac{\overleftarrow{\alpha} F \phi_o}{RT}\right) \qquad [12]$$

where, as before, k_+ is the rate constant, $C_A (n-1)+$ is the concentration of $A^{(n-1)+}$ and $\overleftarrow{\alpha}$ is the anodic transfer coefficient. The net current density i is therefore

$$i = i_+ + i_- = k_+ (C_A (n-1)+) \exp\left(\frac{\overleftarrow{\alpha} F \phi_o}{RT}\right) - k_- (C_A n+) n_s \exp\left(\frac{-\overrightarrow{\alpha} F \phi_o}{RT}\right) \qquad [13]$$

For reasonably concentrated solutions, the potential drop in the diffuse part of the double layer may be neglected, i.e. the ionic concentrations are potential-independent and may be included in the exchange current, i_o, defined here as that current which flows equally in both directions at the potential of zero current and given by

$$i_o = k_+ (C_A (n-1)+) \exp\left(\frac{\overleftarrow{\alpha} F \phi_o^\circ}{RT}\right) = k_- (C_A n+) n_s^\circ \exp\left(\frac{-\overrightarrow{\alpha} F \phi_o^\circ}{RT}\right) \qquad [14]$$

where ϕ_o° and n_s° are the values of ϕ_o and n_s at the potential of zero current, respectively.

The net current density may now be written as

$$i = i_o\left[\exp\left(\frac{\overleftarrow{\alpha}F\eta_H}{RT}\right) - \frac{n_s}{n_s^\circ}\exp\left(\frac{-\overrightarrow{\alpha}F\eta_H}{RT}\right)\right] \qquad [15]$$

where η_H, the Helmholtz layer overpotential is given by

$$\eta_H = \phi_o - \phi_o^\circ \qquad [16]$$

Because of the existence of the semiconductor bandgap, charge transfer may involve either the conduction band or the valence band. The total current is the sum of these contributions. Charge transfer to and from the conduction band occurs by electrons whereas that to and from the valence band involves positive holes. Using [15], expressions for the conduction band and valence band contributions to the current, i_c and i_v respectively, may be written as

$$i_c = i_{co}\left[\exp\left(\frac{\overleftarrow{\alpha}_c F\eta_H}{RT}\right) - \frac{n_s}{n_s^\circ}\exp\left(\frac{-\overrightarrow{\alpha}_c F\eta_H}{RT}\right)\right] \qquad [17a]$$

$$i_v = i_{vo}\left[\frac{p_s}{p_s^\circ}\exp\left(\frac{\overleftarrow{\alpha}_v F\eta_H}{RT}\right) - \exp\left(\frac{-\overrightarrow{\alpha}_v F\eta_H}{RT}\right)\right] \qquad [17b]$$

In the above, the subscripts c and v serve to distinguish terms applicable to the conduction and valence bands, respectively, while p_s is the surface hole concentration with current flowing and p_s° is that with zero net current flowing. The form of [17b] can be better appreciated if the symbolic reaction of equation [9] is rewritten.

$$A^{n+} \rightleftharpoons A^{(n-1)+} + h^{+} \qquad [18]$$

h^+ representing a hole in the valence band.

The present interest has been in the use of p-type semiconductors as photo-cathodes for hydrogen evolution under conditions of reverse bias (negative polarization for a p-type semiconductor). Using semiconductors with relatively large band gaps (> 1 eV), charge transfer at the interface is via the conduction band so that the approximation

$$i = i_c \qquad [19]$$

is quite valid. Such experimental conditions lead to depletion layer (see Figure 2) formation in the semiconductor space charge region.

The potential distribution across a metal-electrolyte interface is easily understood, i.e. because the conductivity of the metal is much greater than that of the electrolyte, the potential drop across the interface occurs exclusively in the electrolyte. For a semiconductor-electrolyte interface, it is more difficult to visualize the distribution of potential. Because a depleted semiconductor is insulator-like, some authors (3, 22) have argued that most of the overpotential occurs in the semiconductor increasing the band bending whereas that in the electrolyte (for reasonably concentrated solutions at least) may be neglected. Others (15, 28) disagree with this view and state that the overpotential in the electrolyte Helmholtz layer is significant and may, in some instances, constitute most or all of the overpotential.

This latter effect is known as Fermi-level pinning. As the name implies it refers to a situation where the semiconductor Fermi level -

and band bending are constant as the applied potential is varied so that the overpotential must be located in the Helmholtz layer. Fermi level pinning usually occurs when a large number of surface states are present on the semiconductor so that its behaviour is metallic (16, 29, 30).

The most general case, that in which part of the overpotential occurs in the semiconductor and part in the electrolyte, as suggested by Myamlin and Pleskov (ref. 27, ch. 2), is considered here. The ~~only~~ simplification adopted, that due to Ahlgren (20, 21), is that the fraction of the overpotential occurring in the Helmholtz layer, ρ, is independent of the overpotential. With this, equations [19] and [17a], the net current density for the situation of interest now becomes

$$i = i_{co}\left[\exp(\overleftarrow{\alpha}_c\rho\Delta) - \frac{n_s}{n_s^o}\exp(-\overrightarrow{\alpha}_c\rho\Delta)\right] \qquad [20]$$

where $\Delta = \eta F/RT$.

For a p-type semiconductor, electrons are the minority carriers, the concentration of which will be significantly altered by illumination. In the absence of current flow, the electron surface concentration, n_s^o, at an illumination intensity I, is related to the electron concentration at the inside edge of the depletion layer of width w, the equilibrium bulk concentration n_o, by $n_s^o = n_o \exp[-(1-\rho)V^oF/RT]$. With current flowing, both the electron surface concentration, n_s, and that at w, n_w, differ from their former values but are similarly related by $n_s = n_w \exp[-(1-\rho)VF/RT]$ where V and V^{ϕ} are, respectively, the potential drop with current flowing and at zero current. From these two expressions (20-23, 26, 31, 32) the ratio n_s/n_s^o is expressible as

$$\frac{n_s}{n_s^o} = \frac{n_w}{n_o} \exp\left[-(1-\rho)\frac{(V-V_o)F}{RT}\right] = \frac{n_w}{n_o} \exp\left[\frac{-\eta_{sc}F}{RT}\right] = \frac{n_w}{n_o} \exp\left[-(1-\rho)\Delta\right] \quad [21]$$

where the overpotential in the space charge region, η_{sc}, is equal to $(1-\rho)\eta$ and to $(1-\rho)(V-V_o)$. As expected qualitatively, a negative applied potential increases the electron population at the surface.

Assuming that the illuminated electrode is in quasi-equilibrium, the following steady-state balance may be written.

$$\begin{bmatrix}\text{net pair generation rate}\\ \text{within the depletion layer}\end{bmatrix} = \begin{bmatrix}\text{minority carrier flux out}\\ \text{of the depletion layer}\end{bmatrix}$$

The left-hand term is the generation rate due to light absorption, minus the recombination rate. The assumption of Dewald (22), that the electron diffusion length (L_n) is much greater than w will be followed, i.e. surface recombination, given by $\nu_s(n_w-n_o)$, where ν_s is the surface recombination velocity, predominates.

From Ahlgren (20), the minority carrier (in this case electron) generation due to light absorption at a depth x into the semiconductor (from the surface), g(x), is

$$g(x) = \int_{E_o}^{\infty} \frac{a(E)W(E,x)dE}{E} \quad [22]$$

where E is the photon energy, a is the absorption coefficient, E_o is the threshold energy for electron-hole pair generation (usually $E_o = E_g$, the semiconductor bandgap energy), and

$$W(E,x) = \left[1-R(E)\right] W_o(E)\exp(-a(E)x) \quad [23]$$

In [23], $W_o(E)$ is the spectral radiation intensity at the surface and R(E) is the surface reflectance. As expected intuitively, W(E,x), the intensity of light of energy E at position x, and hence g(x), decrease as the distance into the semiconductor increases.

Ahlgren next uses the approximation that

$$g(x) = \frac{\bar{a}\gamma I}{e} \exp(-\bar{a}x) \qquad [24]$$

where $\frac{\gamma I}{e}$ and $\bar{a}$ are defined so that [22] and [24] yield the same result. In [24], I is the total light intensity at the surface, γ is a conversion factor from light to electrical energy and $\bar{a}$ is the average absorption coefficient over the appropriate wavelength range.

The minority carrier flux out of the depletion layer is the exiting electron current minus that entering from the bulk by diffusion. The diffusive flux alone, J_n, is given by

$$J_n = -D_n \left(\frac{dn}{dx}\right) \qquad [25]$$

where D_n is the diffusion coefficient for electrons and the differential is evaluated at the inside edge of the depletion layer (i.e. at x = w). Applying Fick's second law, the change in flux with x is obtained as

$$\frac{-dJ_n}{dx} = \frac{dn}{dt} = D_n \frac{d^2n}{dx^2} \qquad [26]$$

The time rate of change of n at a given x is the generation rate plus the rate of increase due to diffusion minus the recombination rate, i.e.

$$\frac{dn(x)}{dt} = g(x) + D_n \frac{d^2n(x)}{dx^2} - \frac{n(x)-n_o}{\tau_n} \qquad [27]$$

where τ_n is the electron's bulk lifetime, related to its diffusion length, L_n, and D_n by

$$D_n = \frac{L_n^2}{\tau_n} \qquad [28]$$

From the quasi-equilibrium (steady-state) assumption we have

$$\frac{dn(x)}{dt} = 0$$

which gives, from [27]

$$\frac{L_n^2}{\tau_n} \frac{d^2n(x)}{dx^2} = -g(x) + \frac{n(x)-n_o}{\tau_n} \qquad [29]$$

Equation [29] is the steady state (electron) continuity equation from which the electron concentration profile, n(x), may be found by solving* [29] with the boundary conditions that $n \rightarrow n_o$ as $x \rightarrow \infty$ and $n = n_w$ at $x = w$. The solution is differentiated and solved for $x = w$ to yield $\vec{J}_n$, where $\vec{J}_n$ is the electron flux entering the depletion layer from the bulk. Note that this flux is in the negative x direction so that there is a sign change from the usual definition ([25]) written for flux in the positive x direction.

---

* The detailed development from equation [27] to equation [32] is given in the Appendix.

$$\vec{J}_n = D_n\left(\frac{dn}{dx}\right)_{x=w} = -\frac{L_n}{\tau_n}(n_w-n_o) + \frac{\bar{a}L_n\gamma I\exp(-\bar{a}w)}{e(1+\bar{a}L_n)} \qquad [30]$$

The minority carrier balance over the entire depletion layer can now be written as

$$\int_o^w g(x)dx - \nu_s(n_w-n_o) = -\frac{i_c}{e} - \vec{J}_n \qquad [31]$$

remembering that i_c is negative since the photo-cathodic current of a reverse-biased electrode is being considered. Using [30] and [24], [31] can be solved (see the Appendix) to yield

$$\frac{n_w}{n_o} = \frac{i_c + \gamma I\left[1-\frac{\exp(-\bar{a}w)}{(1+\bar{a}L_n)}\right]}{en_o\left(\nu_s+\frac{L_n}{\tau_n}\right)} + 1 \qquad [32]$$

This expression can be simplified by recognizing (see references (31) and (22)) that

$$\phi_s = 1-\frac{\exp(-\bar{a}w)}{1+\bar{a}L_n} \text{ and } i_s = en_o\left(\nu_s+\frac{L_n}{\tau_n}\right) \qquad [33]$$

where ϕ_s and i_s are the saturation values, respectively, of the quantum yield and of the dark current (with both surface and bulk generation of electrons considered). Equation [32] then becomes,

$$\frac{n_w}{n_o} = 1 + \frac{i_c+\gamma\phi_s I}{i_s} \qquad [34]$$

Combining [34], [20] and [21] gives

$$i = i_{co}\{\exp(\overleftarrow{\alpha}_c\rho\Delta) - \left[1 + \frac{i_c + \gamma\phi_s I}{i_s}\right]\exp\left[-(1-\rho)\Delta\right]\exp(-\overrightarrow{\alpha}_c\rho\Delta)\} \quad [35]$$

Recalling [19], i.e. $i = i_c$ for the situation of interest here, [35] can be solved for i to give [36],

$$i = -\frac{\gamma\phi_s I}{\frac{i_s}{i_{co}}\exp\left[(1-\rho+\overrightarrow{\alpha}_c\rho)\Delta\right] + 1} + \frac{i_{co}\left[\exp(\overleftarrow{\alpha}_c\rho\Delta) - \exp\{-(1-\rho+\overrightarrow{\alpha}_c\rho)\Delta\}\right]}{1 + \frac{i_{co}}{i_s}\exp(-(1-\rho+\overrightarrow{\alpha}_c\rho)\Delta)} \quad [36]$$

the current-overpotential relationship for hydrogen evolution at an illuminated reverse-biased p-type semiconductor cathode.

Although [36] is somewhat unwieldy, useful relationships are obtained from it by comparing it with [37],

$$i = -\gamma\phi(\eta)I + i_d(\eta) \quad [37]$$

the exact expression for the current in terms of the dark current, i_d, and the quantum yield, ϕ, both of which are functions of η. The negative sign in [37] is required to give the photocurrent contribution to i the correct sign, since i is a cathodic current.

From the aforementioned comparison

$$\phi(\eta) = \frac{\phi_s}{\frac{i_s}{i_{co}}\exp\left[(1-\rho+\overrightarrow{\alpha}_c\rho)\Delta\right] + 1} \quad [38]$$

$$i_d(\eta) = \frac{i_{co}\left\{\exp(\overleftarrow{\alpha}_c\rho\Delta) - \exp\left[-(1-\rho+\overrightarrow{\alpha}_c\rho)\Delta\right]\right\}}{1 + \frac{i_{co}}{i_s}\exp\left[-(1-\rho+\overrightarrow{\alpha}_c\rho)\Delta\right]} \qquad [39]$$

Manipulation of [38] leads to [40], the general

$$\ln\left(\frac{\phi}{\phi_s-\phi}\right) = \ln\frac{i_{co}}{i_s} - \frac{(1-\rho+\overrightarrow{\alpha}_c\rho)F\eta}{RT} \qquad [40]$$

relation derived by Ahlgren [21], which enables the determination of i_{co} from the intercepts of plots of $\ln(\phi/(\phi_s-\phi))$ versus η. Such plots will be termed Ahlgren plots. The slope of an Ahlgren plot, $(1-\rho+\overrightarrow{\alpha}_c\rho)F/RT$, contains two unknowns, ρ and $\overrightarrow{\alpha}_c$, and can give meaningful information only if $\overrightarrow{\alpha}_c$ or ρ is accurately known from some other investigation. Ahlgren (21) assumed $\overrightarrow{\alpha}_c$ could be evaluated from the slope on the basis of a simplifying assumption, namely $\rho = 1$, which is unlikely to be generally applicable.

From [37] it is obvious that $\phi(\eta)$ can be evaluated from the slope of a current density-light intensity plot at constant overpotential, i.e.

$$\phi(\eta) = -\frac{1}{\gamma}\left.\frac{\partial i}{\partial I}\right|_{\eta} \qquad [41]$$

Since it is the ratio $\phi/(\phi_s-\phi)$ which must be evaluated for use in [40] it suffices to evaluate $\frac{\partial i}{\partial I} = (-\gamma\cdot\phi)$ because γ will disappear when the ratio is taken and need not be evaluated explicitly. The value of ϕ_s is found from [41] by choosing η in the plateau (saturation) region of the current density-overpotential curve. The saturation value of the dark current, (i_s), is found from the plateau region of dark current density-overpotential curves.

The definition of overpotential, η, in particular the potential with respect to which it is measured, is a point requiring clarification. For a noble metal electrode in an acidic or basic aqueous solution, hydrogen evolution begins when the electrode potential is cathodic to the $H_3O^+_{(aq)}/H_2$ redox potential in the electrolyte being studied. The choice of this potential as that with respect to which the overpotential should be measured is obvious. For an illuminated semiconductor electrode the choice is less clear.

Since illumination is capable of promoting electrons from the valence band of a semiconductor to its conduction band, reduction of H_3O^+ should theoretically be able to proceed at the flat-band potential (see p. 6-8), provided the conduction band edge of the semiconductor at the interface is above the energy of the H_3O^+/H_2 couple. This is true for the three semiconductors studied in this work, as seen in Figure 3.

If the bands are flat, however, electron-hole separation is unlikely to occur so that one might reasonably expect some degree of band bending to be required to enable light-generated electrons to reach the interface and reduce H_3O^+ without first being annihilated by recombination with holes. There is also the problem of surface recombination of electrons and holes: even more bending is required for a sufficient supply of electrons to reach the surface so that not all are lost by recombination. (Increased band bending increases the ratio n_s/n_o as can be seen from [21], remembering that η is negative.)

One envisages, then, a situation like that in Figure 4, showing the energy levels at a semiconductor-electrolyte interface at the potential

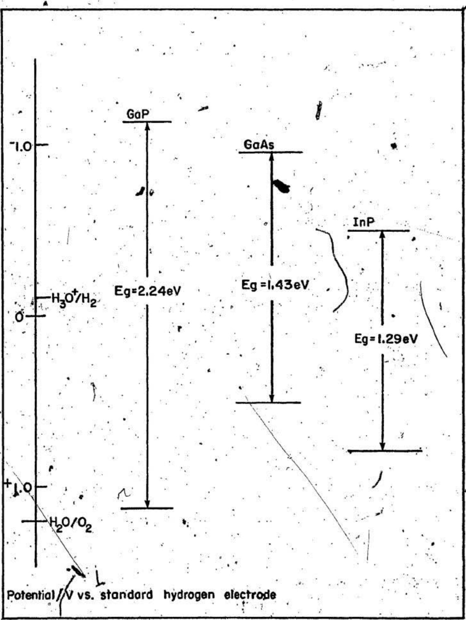

Figure 3. The band gap energies (E_g) and the positions of the conduction and valence band edges in 0.5 M H_2SO_4 for the 3 semiconductors studied in this work. The positions of the H_3O^+/H_2 and H_2O/O_2 redox couples are also shown (after Dare-Edwards et al. (12)).

Figure 4. The illuminated semiconductor-electrolyte interface at the potential of zero current (a), and reverse biased with cathodic current flowing (b), showing the potential distribution across the interface. E_C and E_V are the conduction and valence band edges, V_B and V_H are the band bending and Helmholtz layer potential drop and η_{SC} and η_H the portions of the overpotential occurring in the semiconductor and the Helmholtz layer, respectively.

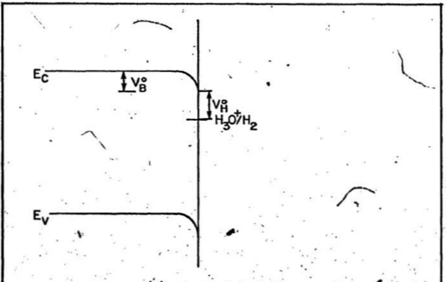

(a) at potential of zero current

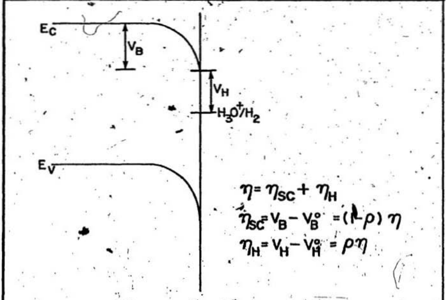

$$\eta = \eta_{SC} + \eta_H$$
$$\eta_{SC} = V_B - V_B^\circ = (1-\rho)\,\eta$$
$$\eta_H = V_H - V_H^\circ = \rho\eta$$

(b) reverse biased

of zero net current under illumination, i.e. there is a well defined band bending, $V_B^{\,o}$, and Helmholtz layer potential drop, $V_H^{\,o}$, at this potential.

The overpotential can now be defined, in the same sense as Horowitz* (33), as the difference between the potential drop across the interface with current flowing, V, and that at the potential of zero current, V^o, i.e.

$$\eta = V - V^o = (V_B - V_B^{\,o}) + (V_H - V_H^{\,o}) \qquad [42]$$

where V_B and V_H are the band bending and the potential drop across the Helmholtz layer, respectively, with current flowing. Note that V_B, V_H, $V_B^{\,o}$ and $V_H^{\,o}$ are negative so that η will also be negative, in agreement with the convention followed here. This definition agrees with that given in Ahlgren's thesis (21).

The above is not the only way that the overpotential at a semiconductor electrode has been defined. Ahlgren elsewhere (20) chose the same convention as for metals and measured η with respect to the H_3O^+/H_2 redox potential. The "exchange" current, by this definition, would be determined at a potential far from the potential of zero current for the semiconductors studied here and the validity of the application of the term "exchange current" to the current measured at $\eta = 0$ is questionable. This convention also requires that both negative and positive overpotentials give negative (cathodic) currents. What this definition does give is the current flowing at the potential

---

* His approach is the same but he neglects the Helmholtz layer potential difference.

at which H_2 evolution would begin on a metal like platinum, a useful number but definitely not what is generally conceived as the exchange current density.

Strictly, one might argue that the flatband potential is the reference point with respect to which the overpotential should be measured since it is the potential at which current should begin to flow in the light. Some researchers (34) have chosen this convention. As discussed previously, however, cathodic current does not begin to flow at this potential and, in fact, anodic (light-independent) current has been observed to flow (12) in the potential regime

$$E^o < E < E_{FB} \qquad [43]$$

where E^o is the observed potential of zero current at a given light intensity. If this reference point were used, the current-potential relationships derived here would have to yield an anodic current for a certain range of negative overpotential, a possibility precluded by the definitions and simplifications used in determining them.

For the theory as developed here, the first definition,

$$\eta = (V_B - V_B^o) + (V_H - V_H^o) = \eta_{sc} + \eta_H = E_i - E^o \qquad [44]$$

where E_i is the potential at which the potential drop across the interface is $V_B + V_H$ and both E_i and E^o are measured with respect to some convenient reference electrode, is most readily applicable. The exchange current obtained using it tells one how "active" the semiconductor surface is at the potential of zero current, in accord with the usual picture. The potentials, E^o, will, in general, be dependent on the type of semiconductor, the light intensity, and the temperature, but, as is explained in the Discussion, the analysis gives exchange current densities (ideally, at least) at the equilibrium potential of the h.e.r. Using E_{FB} as the reference point yields exchange current densities at different potentials since the values of E_{FB} vary with different semiconductors. Ahlgren's convention (20) permits comparison of "exchange" currents at the same potential but it is objectionable for the reasons already cited and for others given in the Discussion. In summary, the definition of [44] seems best suited to this work and will be adhered to.

III. EXPERIMENTAL

Photoelectrochemical Cells

(i) Cells for Photoelectrochemical Measurements at Room Temperature.

A number of different cells, each with slight modifications or improvements for specific purposes, were used in the work. The design was based on one of Ohashi et al. (35) and consisted of a Pyrex body with three compartments, one for each of the reference, counter, and semiconductor electrodes. The compartments were separated by Ace Glass (cat. no. 8192-03) Teflon solution-type stopcocks. The centre (semiconductor electrode) compartment was equipped for illumination with a one inch diameter quartz optical flat, affixed to the cell body with Canadian General Electric silicone sealant. Fine glass frits connected to Ace Glass (cat. no. 8194-19) gas-type Teflon stopcocks permitted gas to be bubbled through each compartment from below.

Later modifications to this basic design included the elimination of inter-compartment stopcocks, inclusion of a glass frit between the semiconductor and counter electrode compartments (to ensure separation of gaseous products) and the replacement of the glass frits at the bottom with ones attached to the caps enabling gas to be supplied from above.

The method of supplying gas was refined even further by a set-up whereby the gas inlets on the caps could be securely attached to glass supply lines via stainless steel bellows (for flexibility) and glass-to-glass Swagelok fittings. A schematic diagram of a typical cell is presented in Figure 5.

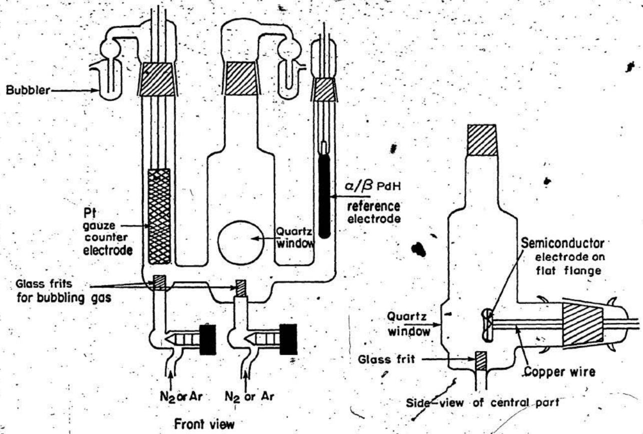

Figure 5. Two diagrams of a typical cell used for room temperature photoelectrochemical experiments.

(ii) The Jacketed Cell

To facilitate construction, this cell consisted of two, rather than three compartments, by making the reference electrode compartment a sidearm off the semiconductor electrode compartment. This change increased the symmetry of the cell and simplified the construction of the jacket.

The electrochemical cell was glass blown within a 10 cm diameter Pyrex tube, sealed at the bottom and around the neck for the electrode holders at the top. Thus almost all of the electrolyte could be surrounded by circulating constant temperature fluid. The exception was the solution in a small neck at the front. A one inch diameter quartz optical flat, through which the semiconductor electrode could be illuminated without absorption by the bath fluid, was attached as before. A mercury-in-glass thermometer used for temperature measurement rested in a glass well dipping into the thermostatic jacket. The well passed into the jacket through a ground joint. The jacket was equipped with inlet and outlet ports for the supply of thermostatted bath fluid. Figures 6a and 6b show two photographs of this cell.

Testing of the temperature recorded by a thermometer in the well, compared to that recorded by one placed near the semiconductor electrode position showed the two measurements to agree to better than 0.1°C. Furthermore the temperature readings were observed to be constant to within ±0.05°C for periods of greater than one hour.

Semiconductor Electrodes - Preparation and Mounting

Specimens of p-GaP, p-GaAs and p-InP were supplied by Metals Research Ltd. (Melbourn, England) as thin slices sawn from ingots. The GaAs was polished on one face. The other materials were smooth but

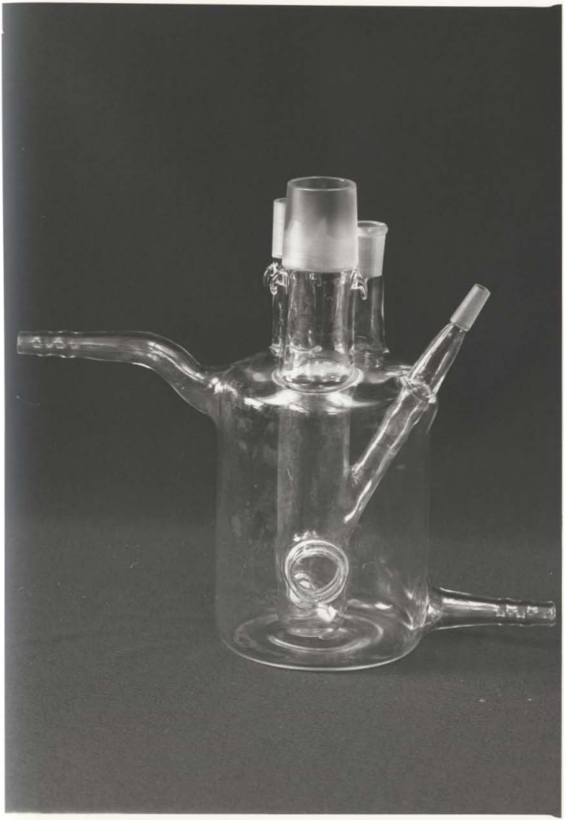

Figure 6a. The jacketed photoelectrochemical cell, showing the quartz optical flat at the front.

Figure 6b. The jacketed photoelectrochemical cell equipped with, front, a semiconductor electrode, to its right, a palladium reference electrode, and behind, a platinum counter electrode.

unpolished. Their properties are summarized in Table 1.

TABLE 1. Some properties of the semiconductor materials used.

p-type Material	Dopant (Zn) Concentration/ atoms·cm^{-3}	Crystal Orientation	Code Letter	Thickness/mm (before etching)
GaP	$1.2 - 1.5 \times 10^{18}$	(100)	W	0.5
GaP	$3.9 - 5.5 \times 10^{17}$	(111)	X	0.4
GaP	$1.2 - 1.5 \times 10^{17}$	(111)	S	0.4
GaAs	$2.1 - 9.4 \times 10^{18}$	(100)	W	0.36
InP	1.3×10^{18}	(111)	-	0.57

The approximately 25-35 mm diameter slices were cut into smaller essentially rectangular pieces using a Fisher brand diamond marking pencil. Specimens selected for use as semiconductor electrodes were first subjected to a chemical etching treatment. Indium phosphide and gallium arsenide samples were etched for 2-3 minutes in a solution of 5% (by volume) Br_2 in methanol (36). After etching they were rinsed with triple-distilled water and allowed to dry in the air.

Gallium phosphide specimens were etched in a mixture of $2HNO_3$:1HCl (by volume) (36) for 10 minutes, rinsed with water, re-etched in the same acid mixture for five minutes, and finally rinsed with water and air-dried.

Once dry, a small cube of 90 wt. % In/10% Zn alloy (36) was attached to one face of each specimen by heating the alloy gently with a 25 watt soldering iron. For (111)GaP and (111)InP samples, the alloy was attached to the etch-pitted (In or Ga) face. The alloy was attached to the unpolished face of the GaAs and to either face of the (100)GaP.

Next, specimens were placed in a quartz tube connected to a vacuum line and heated at ca. 400°C for about 3 hours in an argon atmosphere. The purpose of this heating was to promote diffusion of the zinc in the alloy into the semiconductor, resulting in an "ohmic" contact. That this treatment produced ohmic contacts could be demonstrated by measuring the current-voltage relationship between two such contacts attached to the same semiconductor sample. Linear current-voltage plots (for relatively small applied voltages) were invariably found, as illustrated in Figure 7 for a typical sample.

The specimens were then ready for mounting on glass holders. These holders were of two types - horizontal for earlier cells and vertical for the jacketed cell. As illustrated in Figures 8a and 8b they consisted of a Quadrant Glass Co. flat flange with an opening leading via a tube through an appropriate size glass cone. The vertical holders were also equipped with a gas supply tube terminating in an Ace Glass (ASTM 4-8μ) glass frit, just above the flange.

Electrodes were mounted in the manner of Kohl and Bard (37). First, a suitable length of copper wire was attached to the ohmic contact by heating gently with a 25 watt soldering iron. The wire was then pulled through the tube of the holder and the back of the semiconductor glued to the flat flange with Devcon "five minute epoxy". Finally silicone sealant (C.G.E. or Devcon) was applied around the edges and over the outer part of the exposed front face of the specimen. The silicone sealant was allowed to cure at room temperature for at least 24 h before using an electrode. A mounted electrode is illustrated (in cross-section) in Figure 8c.

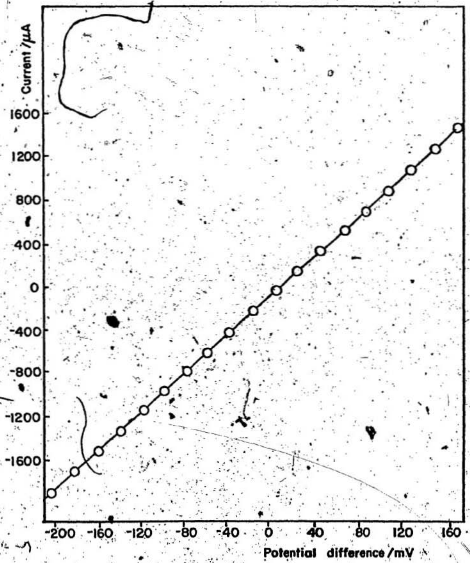

Figure 7. The current-potential difference characteristic for 2 In/Zn alloy contacts on p-GaP.

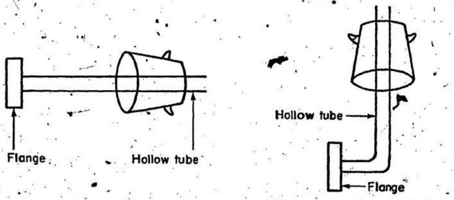

Horizontal semiconductor electrode holder.

8a

Vertical semiconductor electrode holder

8b

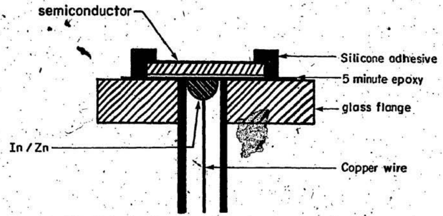

Photoelectrode mounting arrangement

8c

Figure 8. The two types of glass electrode holders used in this work - (a) horizontal and (b) vertical - and the mounting arrangement, in cross-section, (c) for semiconductor electrode specimens on the holders.

Instrumentation

The Light Source Illumination was provided by an Osram 450W high pressure xenon lamp contained within a Photochemical Research Associates (PRA) model ALH 220 arc lamp housing. The lamp was powered by a PRA model 302 power supply, equipped with an ignition unit.

The lamp housing contained a parabolic reflector so that a broad parallel beam of light was emitted. In order to simulate sunlight as closely as possible, the beam was passed through an infrared filter (PRA ALH 1) containing no water. It was then focussed by a quartz lens (PRA ALH 6) onto the cell. A number of neutral density interference filters (Ealing models no. 31-8980-2, 35-6246, 31-9020-440, and 26-8854-2) of absorbances 1.0, 1.5, 2.0 and 3.0 were available for interposition in the light path to reduce its intensity. The light intensity could also be varied over a limited range by adjusting the current setting on the power supply. The lamp, other optical equipment, and the cell or light intensity-measuring probe were all clamped using holders attached to a Lasico 2-metre long aluminum optical rail which was fastened to the bench top. This greatly facilitated alignment of the optical equipment and of the cell with the light beam. The set-up is shown schematically in Figure 9.

The light intensity incident upon the electrode was measured using a Yellow Springs Instruments model 65A radiometer equipped with a probe which could be placed at the electrode position. The intensity was corrected for absorption by the 0.5 M H_2SO_4 in the cell by passing the light through a small aqueous H_2SO_4-filled cell, with path length equal to that of the solution in front of the electrode, interposed between the lamp and the probe.

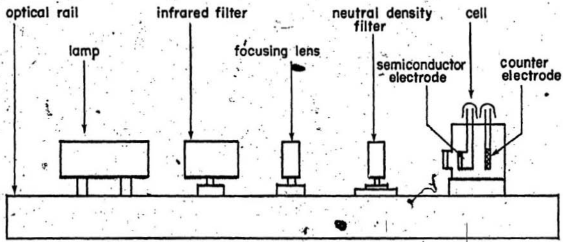

Figure 9. Schematic diagram showing the arrangement of the lamp, other optical equipment, and the cell along the optical rail.

Temperature Control and Variation

A Neslab model RTE-8 circulating constant temperature bath, filled with a 1:1 mixture, by volume, of ethylene glycol and water, was used to thermostat the jacketed cell at various temperatures. Temperature control was precise to ± 0.05°C.

The temperature was measured using an Ertco F series (range -1°C to 51°C) mercury-in-glass thermometer which had previously been calibrated against a platinum resistance thermometer. For temperatures greater than 51°C, a wide range (-10 - 110°C) mercury thermometer (Canlab) was used.

Electrochemical Measurements

Cyclic voltammograms were generated using either a Princeton Applied Research (PAR) model 371 potentiostat-galvanostat or a laboratory-built potentiostat, with an Exact Electronics type 301 function generator, operating at low frequency in the triangular wave mode, connected to the potentiostat auxiliary input. The voltammograms were recorded on a Hewlett-Packard (HP) model 7046A X-Y recorder. Alternatively, slow voltammograms were recorded point-by-point using an HP model 3467A logging multimeter.

Fast (500 mV.s^{-1}) current-potential characteristics were usually produced using the PAR model 174 polarographic analyzer and were recorded on the HP X-Y recorder. Some preliminary fast current-potential plots were made using a Tektronix model 5441 oscilloscope and a Polaroid camera.

The stability of the photocurrent with time at a given potential (using one of the potentiostats) was determined either with an HP model

680M strip chart recorder or the previously mentioned HP logging multimeter.

Materials

Gases. In preliminary work relatively impure (K-grade) nitrogen from Canadian Liquid Air (CLA) was bubbled, without further treatment, through the electrolyte solutions.

In later work, CLA ultra high purity (UHP) argon (< 2 ppm O_2, < 10 ppm N_2, < 1 ppm H_2, < 0.5 ppm H_2O, < 0.5 ppm total hydrocarbons), further purified by passage through pre-reduced BASF-type BTS catalyst (to remove O_2), was bubbled through the solution for pre-saturation. In Figure 10 the gas handling system is depicted. UHP argon was also used as the inert atmosphere for the preparation of the alloy contacts on the semiconductors.

Acids. Except for those used in cleaning, all acids were BDH ARISTAR grade. They were used either undiluted, for etching, or diluted with triple-distilled water to yield electrolyte solutions of suitable concentrations.

Bromine (for etching). Mallinckrodt A.C.S. analytical reagent grade.

Methanol (for etching). Fisher certified A.C.S. - spectroanalyzed.

Triple-distilled water. Tap water was distilled once, re-distilled from alkaline $KMnO_4$ and finally distilled again under nitrogen, carbon dioxide being excluded by use of a soda-lime trap.

Metals

Platinum and palladium. (Used for counter and reference electrodes respectively). Apparatus grade metals (Johnson, Matthey and Mallory (JMM)) were used.

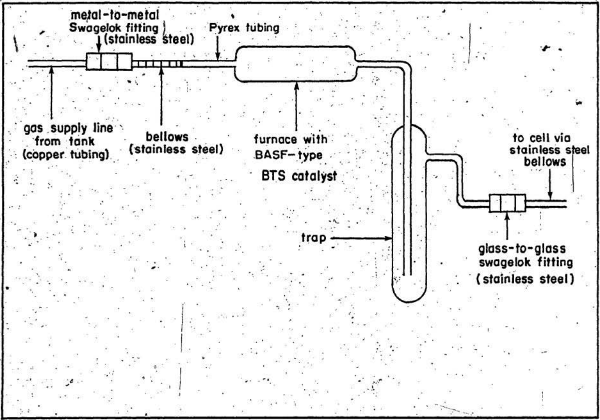

Figure 10. A schematic diagram of the gas handling system for supplying very pure argon td the photoelectrochemical cells.

Indium (for alloy). BDH (99.9% pure) and Fisher (99.97% pure) were used.

Zinc (for alloy). Alfa division of Ventron 99.9999% pure zinc shot was used.

Platinum and palladium compounds (for plating)

$Pd(NH_3)_4(NO_3)_2$ - from JMM (Rh, 7 ppm; Ca, Cu, Fe, Mg, Si, Ag all < 1 ppm; Pd 35.94%)

$Pt(NH_3)_4Cl_2$ - JMM Puratronic grade (Pd, 5 ppm; Fe, 1 ppm; Si, 1 ppm; Ca, Cu, Mg all < 1 ppm)

Reference and counter electrodes

The reference electrodes used consisted of a 3 mm diameter palladium rod welded to a platinum contact wire, the junction being sealed in Pyrex glass (see Figure 11). When charged cathodically at 1.5 $mA.cm^{-2}$ in 0.1 M $HClO_4$ for about 16 hours, hydrogen dissolves in the palladium and an equilibrium between two (α and β) PdH phases is established, maintaining a relatively constant potential. After charging, the electrode worked as an effective reference electrode (potential = 50-60 mV vs standard hydrogen electrode) with reasonable stability, for 3-6 days, after which period the charging process was repeated. Whether or not the electrode was palladized (covered with a fine electrodeposit of palladium metal) seemed to make little difference to its suitability as a reference electrode (see references (38) and (39)).

Counter electrodes were constructed exclusively of platinum gauze wound on a glass rod with external contact via a platinum wire (see Figure 11).

Cleaning

Apparatus received from the glass-blowing shop was invariably

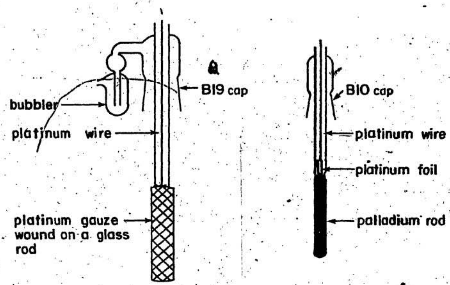

Counter electrode

Reference electrode

Figure 11. Drawings showing the construction of typical counter and reference electrodes used in this work.

cleaned first with saturated aqueous sodium hydroxide. Following thorough rinsing with distilled water, all glassware not containing stainless steel parts or palladium metal was cleaned with hot concentrated nitric acid, rinsed with distilled water and then washed copiously with triple-distilled water, and finally dried in a clean oven.

Glassware with parts sensitive to nitric acid was thoroughly rinsed, after the alkaline treatment, with distilled water and triple-distilled water and dried in the oven.

Methods

(i) Preliminary and Metal-Plating Experiments

Before each run a semiconductor electrode was etched for a short time (usually 60 s for a new electrode and 15 s or 30 s for an electrode which had previously been used). GaP was etched in the $2HNO_3$:1 HCl mixture (36), GaAs in $1HNO_3$:2HCl:$2H_2O$ mixture (40) because it was less vigorous than methanolic bromine, and InP in $2HNO_3$:1HCl:$2H_2O$ mixture (41). After etching, the electrodes were rinsed well with triple-distilled water and then with the electrolyte to be used (almost exclusively 0.5 M H_2SO_4). The wet electrode was placed in the cell which was quickly filled with electrolyte solution. The reference and counter electrodes were then placed in position and the cell aligned so that the light was focussed at the semiconductor electrode position. Nitrogen or argon was bubbled through the electrolyte before experiments and also during experiments when gas supply from above was possible. With gas supplied from below, it was found desirable to discontinue its flow during illumination because of light scattering by gas bubbles. The rest potentials of the semiconductor electrodes in the dark, i.e. in room light but with the lamp off, were usually noted. Certain values proved to be characteristic of a properly functioning electrode (ca. +300 mV* for InP and GaAs and ca. +500 mV for GaP) and rest potentials more than about 200 mV negative of these values indicated either leakage of electrolyte to the back contact of the semiconductor or a poor metal-semiconductor contact.

Cyclic voltammograms of the bare electrode in the dark (dim room light) and with the lamp on, at one or more light intensities, were recorded. This was usually repeated at regular intervals until a stable cyclic voltammogram, i.e. one which exhibited little or no drift with time, was obtained.

Frequently a procedure known as "blank" plating was performed, whereby the electrode was subjected to all of the procedures of the plating treatment except that metal ions were absent. Following this "blank" plating the cyclic voltammogram was again recorded in order to verify that this treatment had had little or no effect on the electrode behaviour. If an effect was observed, the "blank" plating was repeated until it resulted in no further change.

The electrode was then ready for plating. The procedure involved first calculating the volume of a Pt(II) or Pd(II) stock solution required to give the desired noble metal atom surface coverage (usually in the 0.4 – 100 atoms·Å^{-2} range) assuming complete deposition of plating metal. This volume of solution was added to the electrolyte using an Eppendorf pipette. The electrode was next exposed to a light intensity of ca. 100 mW.cm^{-2}, and polarized at a potential just negative of

---

* All potentials are quoted with respect to the α/β PdH reference electrode discussed earlier.

the onset potential for hydrogen evolution on the same bare electrode, to initiate the plating. (For each semiconductor this plating potential was always negative of the Pt^{2+}/Pt and Pd^{2+}/Pd equilibrium potentials). Stirring was effected by bubbling gas through the electrolyte. Plating was usually continued overnight (for ca. 16 h), with the semiconductor electrode illuminated, to ensure that most, if not all, of the metal would be plated out under the diffusion-controlled conditions.

Plating was halted the next day by allowing the semiconductor electrode potential to return to its rest value. Cyclic voltammograms were then recorded at regular intervals until they became reproducible.

The stability of the bare and plated electrodes was compared by measuring the time dependence of the photocurrent with the semiconductor electrode polarized at a particular potential at which the current was initially relatively large, but the applied cell voltage still small enough so that the overall energy conversion efficiency was positive (i.e. the applied voltage was less than 1.48 V (see equation [2], Chapter II). The energy conversion efficiency was calculated using [2] from measurements of applied cell voltage, current and light intensity.

(ii) Photoelectrochemical Kinetics Experiments

a) Non-thermostatted conditions. The preliminary treatments, i.e. the etching and rinsing of semiconductor electrodes and the alignment and filling of the cell were exactly as in the previous experiments.

Current-potential characteristics were recorded at a fast rate (500 $mV.s^{-1}$) starting at or near the steady-state potential and proceeding in a negative direction at least as far as necessary to reach a limiting current plateau. Fast scans were used (taking 2-3 s to complete) on the premise that they could be completed before the electrode surface condition was significantly altered, presumably by the build-up and adsorption of intermediates or products which could act as electron-hole recombination centres and result in lowered currents. The effect of scanning speed can be seen in Figure 12 which shows current-potential scans recorded at various scan rates.

Generally, 1-2 days in solution were required before the semiconductor electrode exhibited reproducible current-potential characteristics at a given light intensity. Presumably, freshly etched electrodes required some time in solution before the surface attained equilibrium (see Figure 13). The irreproducibility of newly etched surfaces has also been reported recently by Albery and Bartlett (42) for GaP, although they found it necessary to wait only an hour or so.

Once a stable surface had been achieved, data collection for the kinetics measurements was started. Fast current-potential characteristics were measured at several (usually 4 or 5) different incident light intensities. These were then analyzed as outlined in Chapter II (see equations [40] and [41]) and the kinetic parameters elucidated. The current-light intensity and Ahlgren plots were each analyzed by subjecting them to linear least squares regressions.

Saturation dark current (i_s) values, required for the analysis, were obtained from the middle of the plateau region of fast current-potential characteristics recorded in the dark, i.e. with the cell covered with dark cloth, the room darkened with blinds and fluorescent lights off.

In the above experiments, the temperature of the electrolyte was assumed to be room temperature: 23 ± 1°C.

Figure 12. The effect of the potential scan rate on the current-potential characteristic for hydrogen evolution on illuminated p-GaP in 0.5 M H_2SO_4. Light intensity = 140 $mW.cm^{-2}$. The scan rates were: (1) 10 $mV.s^{-1}$; (2) 100 $mV.s^{-1}$; (3) 500 $mV.s^{-1}$.

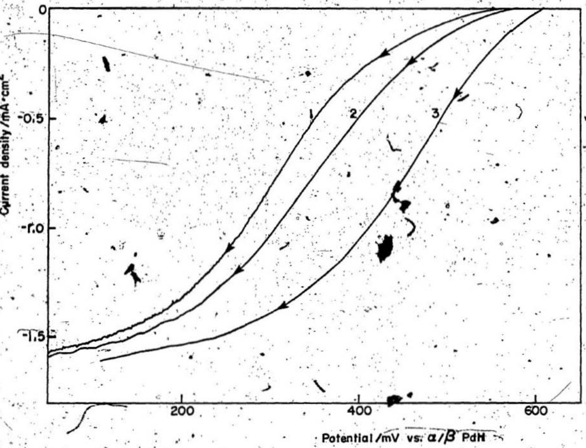
0
-0.5
-1.0
-1.5
Current density /mA·cm^{-2}
200
400
600
Potential /mV vs. α/β PdH
1
2
3

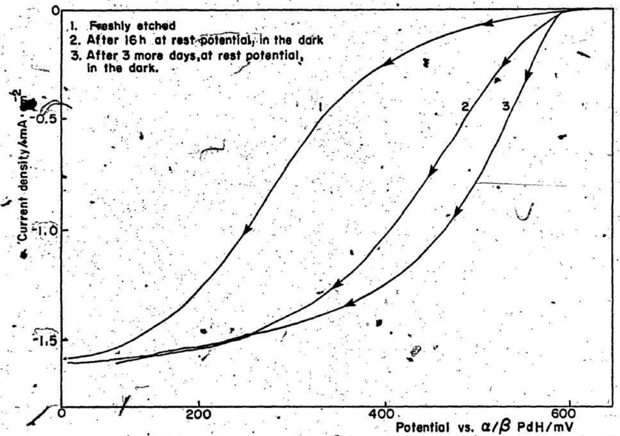

Figure 13. The effect of total time in solution on the current-potential characteristic for hydrogen evolution on illuminated p-GaP in 0.5 M H_2SO_4. Light intensity = 140 mW.cm^{-2}. Electrode condition given in inset.

b) Thermostatted conditions. The preliminary etching and rinsing of the semiconductor electrodes, as well as the mounting and alignment of the cell, were done exactly as before. Now, however, with the semiconductors mounted on vertical-type holders, the cell could be filled with the electrolyte and the reference and counter electrodes positioned before the semiconductor electrode was lowered into the cell. Again, a day or so was required before results with the semiconductor electrode were reproducible.

After this waiting period, data collection, which now required at least 12 hours, often spread over two days, was begun. With the cell thermostatted at a particular temperature by use of the circulating bath, fast current-potential characteristics were recorded at 4 or 5 different light intensities. The bath was then set for a new temperature, and, after waiting at least thirty minutes for the bath to reach this temperature (to ensure that the electrolyte temperature did not lag behind), current-potential characteristics at several light intensities were recorded for the second temperature. This whole procedure was repeated until 4 or 5 different temperatures in the range 2°C - 65°C had been studied. A duplicate set of measurements at one of the first studied temperatures was usually carried out at the end of the sequence to verify the reproducibility of the results. During the time required for measurements at one temperature, temperature variations of $\leq \pm$ 0.05°C were observed.

From the values of the exchange current densities obtained at different temperatures by the analysis outlined in Chapter II, the enthalpies of activation, $\Delta H^{\ddagger}$, and the logarithms of the pre-exponential factor, $A^{\ddagger}$, were obtained, respectively, from the slope and intercept of the Arrhenius plot of $\ln(i_{co})$ vs $1/T$, where

$$\Delta H^{\ddagger} = -R\left\{\frac{\partial \ln(i_{co})}{\partial(1/T)}\right\} \quad [45]$$

and $$\ln A^{\ddagger} = \ln(i_{co}) \text{ evaluated at } 1/T = 0 \quad [46]$$

Weighted least squares analysis, with weights equal to the inverse square of the standard deviations, was used in the treatment of the Arrhenius plot data.

IV. RESULTS

1. Preliminary Studies and Noble Metal Plating Experiments.

a. Gallium phosphide

Because it has the most positive onset potential for hydrogen evolution of the three semiconductors studied, gallium phosphide was the subject of the most extensive research in this part of the work. In Figure 14, representative current-potential curves for hydrogen evolution on GaP and GaAs are shown. The current densities at saturation are larger on GaAs (as is to be expected because of its smaller band gap) but the cathodic onset is about 700 mV negative to that for GaP. For InP, the threshold potential is near to that of GaAs and the current densities are comparable, but cathodic polarization also caused special problems (see (c) below).

Although GaP was promising in that hydrogen evolution began some 500-600 mV positive of the equilibrium potential of the H_3O^+/H_2 redox couple, the current densities were small and consequently the overall energy conversion efficiencies (equation [2], Chapter II) were small, ca. 0.01%. Various anodic and cathodic polarization treatments had little influence on the shape of the current-potential curves or on the efficiency.

The electrodeposition of thin films of platinum and palladium did, however, result in favourable (positive) shifts of the GaP current-potential characteristics (see Figure 15 for a typical result). This effect had been reported by Nakato et. al. (17) for metal coverages of 0.2-2 atoms.$Å^{-2}$. Here the investigation was extended to include

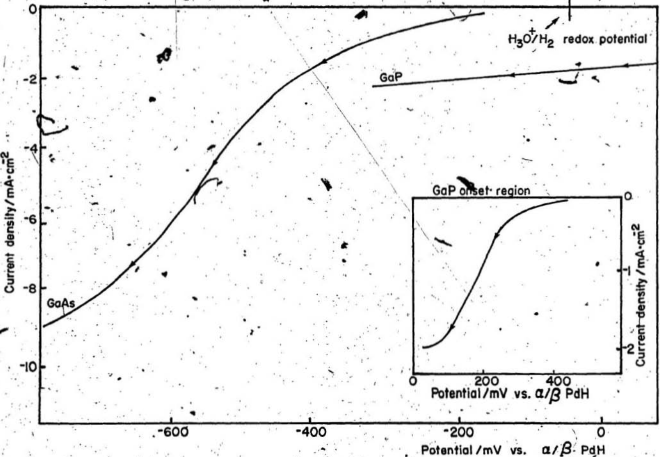

Figure 14. Representative current-potential curves for hydrogen evolution on illuminated p-GaP and p-GaAs in 0.5 M H_2SO_4. Light intensity = 150 mW.cm^{-2}. Inset: GaP onset region.

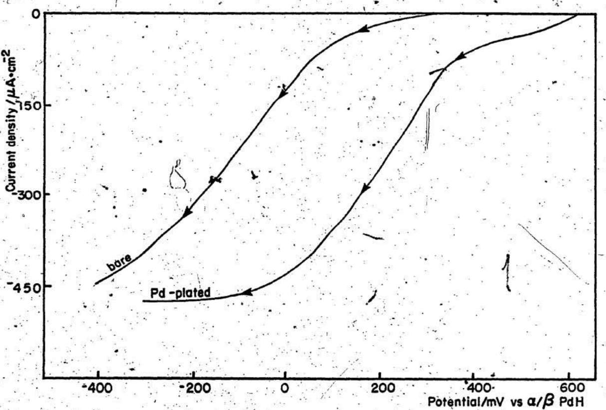

Figure 15. The effect of plating 40 atoms.Å^{-2} of palladium on the current-potential characteristic for hydrogen evolution on illuminated p-GaP in 0.5 M H_2SO_4. Light intensity = 150 mW.cm^{-2}.

platinum and palladium coverages from 0.2-100 atoms.Å^{-2}. Up to a coverage of ca. 40 atoms.Å^{-2}, increased coverages resulted in larger shifts of the current-potential characteristics. Beyond this level additional plating provided no beneficial effect and at very high metal coverages (> 100 atoms.Å^{-2}) the photoeffect began to diminish and the current-potential curves exhibited metallic behaviour.

In the "useful" range studied, 0.4-40 atoms.Å^{-2}, stability studies (photocurrent vs time at a constant potential or cell voltage) showed that GaP electrodes with the largest metal atom coverages, and hence the most favourable current-potential characteristics, exhibited the poorest stability (Figure 16). Gallium phosphide plated with 4 atoms.Å^{-2} of palladium showed intermediate stability while that with the lowest coverage had the best stability. This most stable electrode, for which $\xi = 0.015$, was only about 50% more energy-efficient than the bare electrode. The best initial improvement, for GaP electrodes plated with 40 atoms.Å^{-2} of noble metal, gave $\xi = 0.02$, but the enhancement quickly diminished (Figure 16). Bare and lightly-plated GaP electrodes showed quite good long term photocurrent stability (24 h or better).

When platinum was plated instead of palladium, the results were quite similiar. The maximum stable energy conversion efficiency observed, for GaP with ca. 0.4 atoms.Å^{-2} of platinum, was 0.03%. The above results will be considered further in the Discussion.

b. Gallium arsenide

As already mentioned, the cathodic onset potential for hydrogen evolution on illuminated unplated p-GaAs is negative with respect to the H_3O^+/H_2 equilibrium potential. The aim of plating was to shift the current-potential curve sufficiently so that the onset would occur

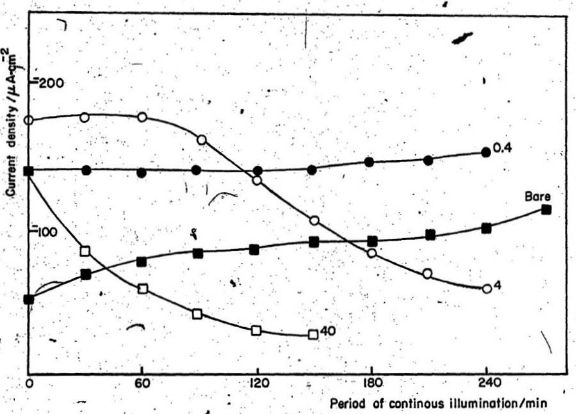

Figure 16. Stability (time variation of current at constant potential (+200 mV vs. α/β PdH)) for hydrogen evolution on illuminated p-GaP (bare and plated with various amounts of palladium) in 0.5 M H_2SO_4. The numbers at the end of each curve indicate metal coverage in atoms.Å^{-2}. Light intensity = 80 mW.cm^{-2}.

at positive potentials. As Figure 17 reveals, plating of a small amount of platinum did result in a fairly large positive shift both of the current-potential curve and the onset, but there was still very little cathodic photo-current at potentials positive to the H_3O^+/H_2 equilibrium potential. Figure 17 shows the largest improvement achieved in experiments in which various amounts (0.4-100 atoms.$\AA^{-2}$) of platinum or palladium were plated on GaAs. Higher metal coverages (100 atoms.$\AA^{-2}$ or more) usually resulted in metal-like current-potential behaviour.

Thus, although plating of small amounts of platinum and palladium on GaAs did result in a considerable shift of the current-potential characteristics, other problems with GaAs result in such a delayed onset for cathodic current that it is unlikely to be useful in efficient photo-assisted electrolysis of water. This problem has also been recognized by Fan and Bard (16).

c. Indium phosphide

As mentioned previously, cathodic polarization of InP resulted in unusual behaviour. Successive cyclic voltammograms were rarely reproducible and, if the electrode was maintained at a sufficiently negative potential (ca. -1 V) for even as short a period as 1 minute, a whitish film formed on the InP surface. This had previously been observed by Mayumi et al. (43) and was confirmed by Uosaki (36) and Uosaki and Kita (44) for cathodic polarization of p-InP in 0.5 M H_2SO_4. Mayumi et al. determined from ion microanalyzer measurements that the film was indium metal formed presumably by the cathodic decomposition of InP.

As a result of this film formation, anodic scans performed immediately after cathodic scans showed distinct anodic current

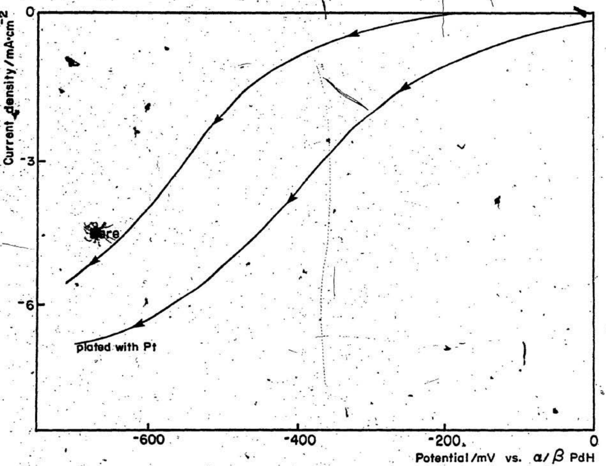

Figure 17. Best shift of the current-potential characteristic for hydrogen evolution on illuminated p-GaAs in 0.5 M H_2SO_4, obtained by plating 0.4 atoms.Å^{-2} of platinum. Light intensity = 150 mW.cm^{-2}.

peaks. The height of these peaks increased with the duration of the preceding cathodic polarization as also found in (44). The film was also observed to form in the dark, at negative potentials, but the rate of film formation was greatly increased by illumination, i.e. its formation depended upon the electron supply at the InP surface. These findings will also be reconsidered in the Discussion.

The only way, then, to achieve reproducible current-potential relationships with InP was to ensure that this film had been completely removed before repeating scans. This could be accomplished by subjecting the film-covered InP to short-duration anodic pulses (100-200 mV positive of the rest potential for ca. 30 s).

A few platinum plating experiments performed with InP resulted in positive shifts of the current-potential characteristic but did not result in very large currents at potentials positive to the H_3O^+/H_2 equilibrium potential. The presence of platinum did, however, greatly inhibit film formation, presumably by making hydrogen evolution the favoured reaction (see the Discussion).

d. Summary

The presence of thin electrodeposits of platinum or palladium on the surface of GaP, GaAs and InP results in favourable, i.e. positive potential, shifts of their current-potential characteristics for hydrogen evolution under illumination. For GaAs and InP, however, the shifts are inadequate to overcome other problems (such as electron-hole recombination) and the currents remain quite small at potentials positive to the H_3O^+/H_2 equilibrium potential, resulting in very small or even negative energy conversion efficiencies.

2. Photoelectrochemical Kinetics Measurements

i. Preliminary work

Preliminary experiments for all three semiconductors made use of an unjacketed cell, so measurements were limited to room temperature, with temperature control no better than ± 1 K. The purpose of these investigations was to determine how well the data conformed to equation [40] (Chapter II).

a. Gallium phosphide

Two experiments were done with this material as the electrode and although each separately fitted the theory well, the exchange current densities obtained were in poor agreement (Table 2). The strong light intensity-dependence of the current-potential curves for hydrogen evolution is demonstrated in Figure 18. From these curves, values of current density and light intensity at several overpotentials were extracted and plotted, as shown in Figure 19. These current density-light intensity plots exhibited good linearity and the anticipated increase of slope from the cathodic onset to the plateau region of overpotential. Using equation [37] from Chapter II, values of $\phi \cdot \gamma$ and $\phi_s \cdot \gamma$ were calculated at appropriate overpotentials and used to plot $\ln(\phi/(\phi_s-\phi))$ vs. η (Figure 20). The intercept at $\eta = 0$ of this latter plot yields the quantity $\ln(i_{co}/i_s)$. Since i_s is easily determined (from current-potential scans in the dark) the value of $\ln(i_{co})$ can then be computed.

Figure 20 also shows that provided one does not select points too near the plateau region, the standard deviations of the points are of comparable magnitude. For points near the plateau region, $\phi \to \phi_s$ or $\phi_s - \phi \to 0$ and the calculated errors in $\ln(\phi/(\phi_s-\phi))$ increase rapidly.

Table 2. A summary of the results of the preliminary photoelectrochemical experiments with GaP, GaAs and InP. T = 297 ± 1 K.

Semiconductor	Trial No.	$\ln(i_{co}/i_s)$	i_s/µA.cm^{-2}	$\ln(i_{co}$/µA.cm$^{-2})$
GaP	1	-1.49(±0.09)[1]	0.36	-2.52(±0.09)[2]
GaP	2	-2.78(±0.13)	0.36	-3.80(±0.13)
GaAs	1	-4.62(±0.12)	10	-2.32(±0.12)
GaAs	2	-5.07(±0.08)	10	-2.77(±0.08)
InP	1	-4.44(±0.18)	2.0	-3.74(±0.18)
InP	2	-5.00(±0.49)	2.0	-4.31(±0.49)

[1] Unless otherwise indicated, the uncertainties reported are the calculated standard deviations.

[2] Since the relative error in i_s is much smaller than that in $\ln(i_{co}/i_s)$, the relative error in $\ln(i_{co})$ is the same as that in $\ln(i_{co}/i_s)$.

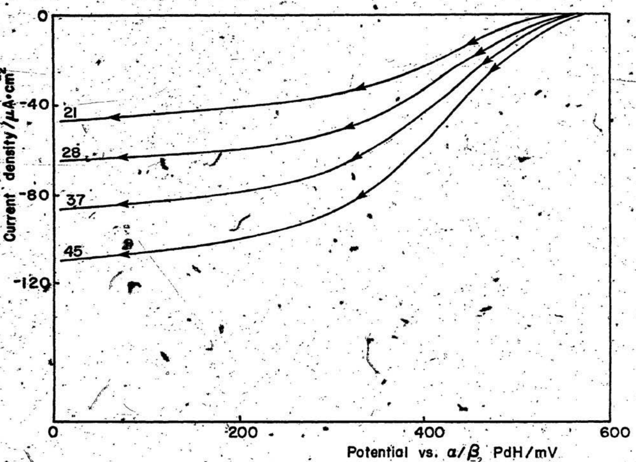

Figure 18. The effect of light intensity (given above each curve in mW. cm^{-2}) on the current-potential characteristic for hydrogen evolution on p-GaP in 0.5 M H_2SO_4. T = 297 ± 1K.

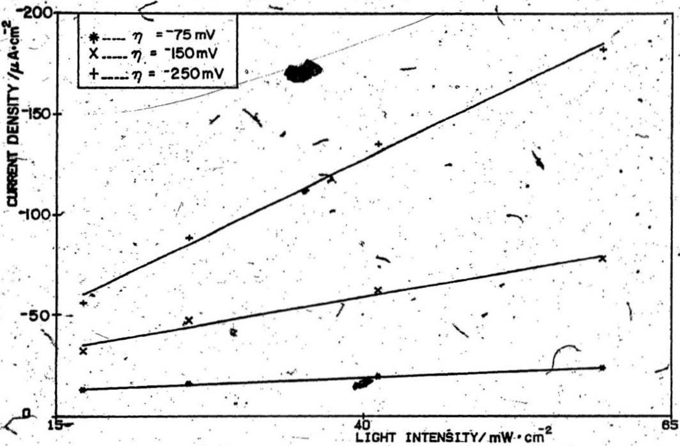

Figure 19. Representative current density vs. light intensity plots at several values of η for hydrogen evolution on p-GaP in 0.5 M H_2SO_4.

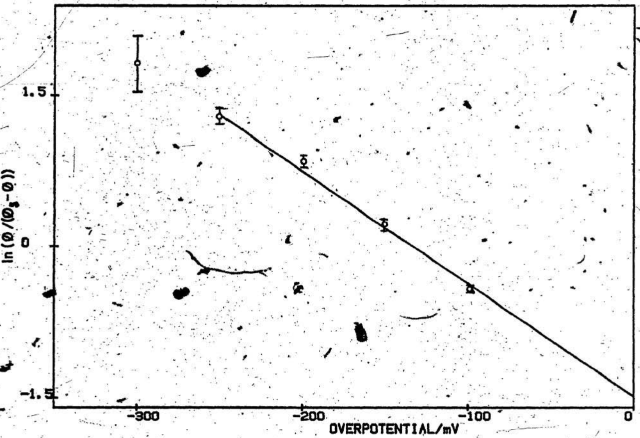

Figure 20. An Ahlgren plot for hydrogen evolution on illuminated p-GaP in 0.5 M H_2SO_4 (for data of Figures 18 and 19). T = 297 ± 1 K.

Therefore the errors in the y-intercepts of the Ahlgren plots were calculated using ordinary least squares analysis, omitting any points in or near the plateau region for which the errors were inordinately large.

The values calculated for $\ln(i_{co})$ were of the same order of magnitude as those found later at comparable temperatures in the variable temperature experiments.

b. Gallium arsenide

The calculated values of the exchange current density for hydrogen evolution in two experiments on illuminated GaAs agreed reasonably well (Table 2). The experimental data (i.e. the current-potential curves at several light intensities (Figure 21)) were treated exactly as for GaP. A typical current density-light intensity plot (Figure 22) and Ahlgren plot (Figure 23) are presented. They exhibit good, if not excellent, linearity. The values of $\ln(i_{co})$ obtained agreed well with those obtained in the same temperature range in the later work with the thermostatted cell.

c. Indium phosphide

With InP, the calculated values of the exchange current density from the two preliminary trials also did not agree particularly well (Table 2). The current density-light intensity plots (Figure 25), taken from the current-potential curves at various light intensities (Figure 24), and the Ahlgren plots (Figure 26) did, however, show quite reasonable linearity for both trials. The values of $\ln(i_{co})$ obtained were somewhat larger than those calculated in the same temperature range in the later variable temperature work.

d. Summary

The reproducibility of the results for each semiconductor from

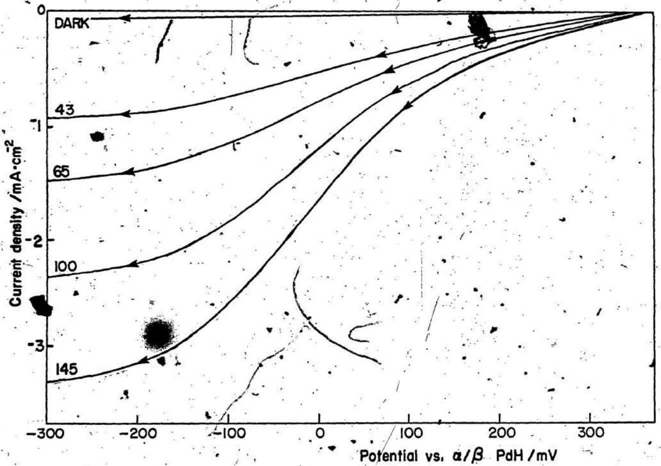

Figure 21. The effect of light intensity on the current-potential characteristic for hydrogen evolution on p-GaAs in 0.5 M H_2SO_4. The numbers on each curve give the light intensity in mW.cm^{-2}.

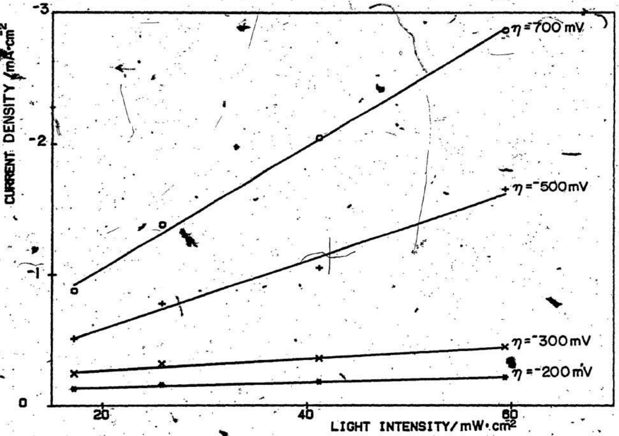

Figure 22. Typical current density vs. light intensity plots at several overpotentials (indicated at the end of each plot) for hydrogen evolution on p-GaAs in 0.5 M H_2SO_4.

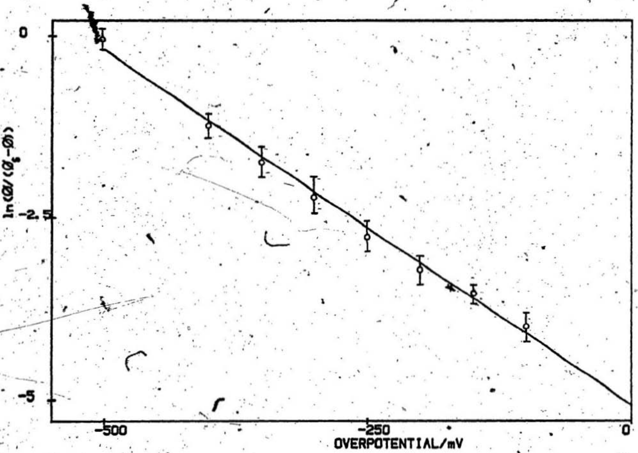

Figure 23. Ahlgren plot for hydrogen evolution on illuminated p-GaAs in 0.5 M H_2SO_4. T = 297 ± 1 K.

Figure 24. Current-potential characteristics in the dark and at several light intensities (indicated above each curve in mW.cm^{-2}) for hydrogen evolution on p-InP in 0.5 M H_2SO_4. T = 297 ± 1 K.

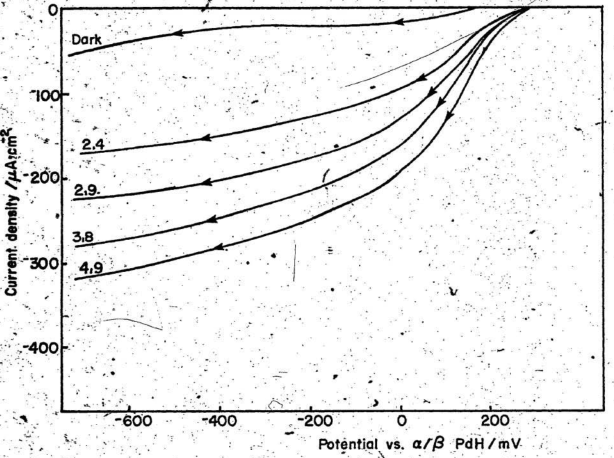
0
-100
-200
-300
-400
Current density / μA/cm²
Dark
2.4
2.9
3.8
4.9
-600
-400
-200
0
200
Potential vs. α/β PdH / mV

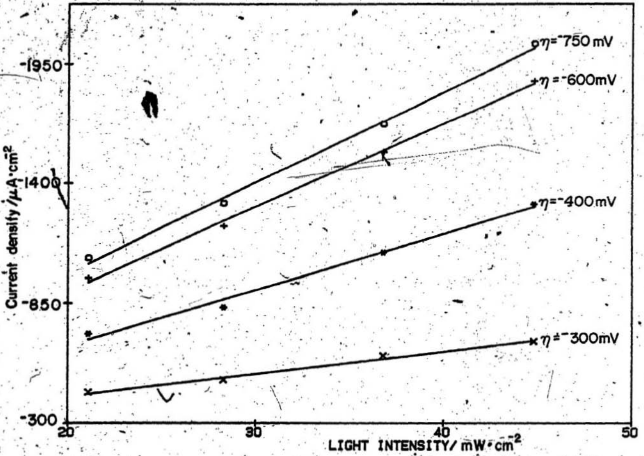

Figure 25. Typical current vs. light intensity plots at several overpotentials (indicated at the end of each plot) for hydrogen evolution on p-InP in 0.5 M H_2SO_4.

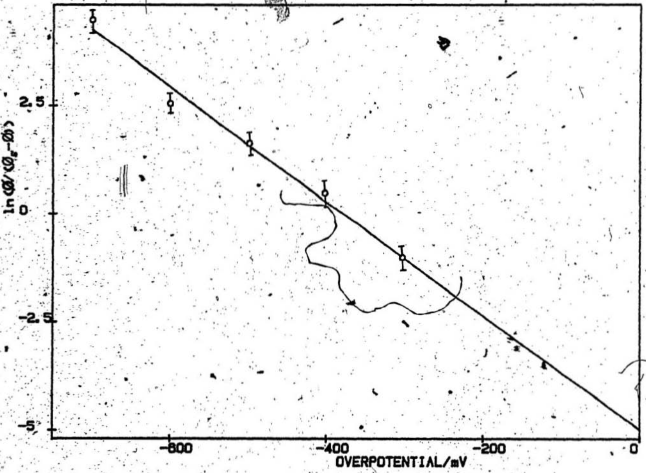

Figure 26. Ahlgren plot for hydrogen evolution on illuminated p-InP in 0.5 M H_2SO_4. T = 297 ± 1 K.

trial to trial was, at best, only fair. This is probably due, in part at least, to the difficulty in maintaining a reproducible (semiconductor) electrode surface condition, a matter which will receive further comment in the Discussion.

Despite the above, and on the basis of the quite reasonable fit of the current density-light intensity plots and the Ahlgren plots to the theoretical expressions, for each trial, it was decided that extension of these experiments to a range of temperatures was desirable.

ii. Variable temperature experiments

In these investigations, use was made of a jacketed photoelectrochemical cell to measure exchange current densities at several carefully controlled (± 0.05 K) temperatures in the 275-340 K region. These results were used to construct Arrhenius plots from which the enthalpies of activation of the hydrogen evolution reaction on the three semiconductors were estimated.

a. Gallium phosphide

Several separate experiments were performed using two different GaP electrodes. As before, current-potential curves recorded at several light intensities constituted one experimental run, and this procedure was repeated at three or four additional temperatures. The dependence of these current-potential curves, at one temperature, on light intensity was demonstrated previously (Figure 18). Figure 27 shows the effect of temperature on the current-potential characteristics at constant light intensity.

For each temperature, the current-potential data were analyzed as before (part (i)). Typical current/density-light intensity plots for several overpotentials at one temperature are shown in Figure 28.

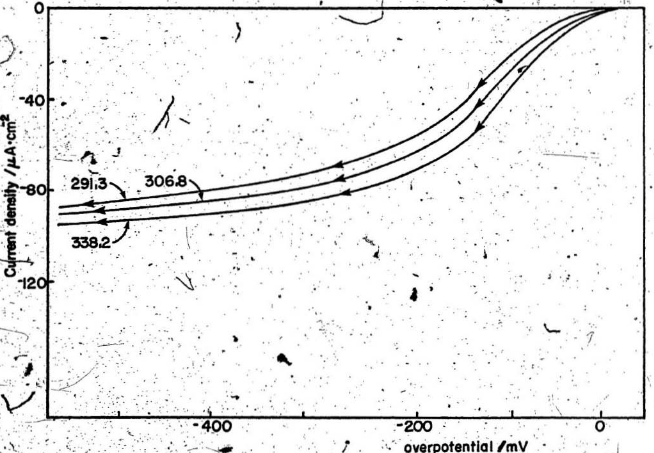

Figure 27. The effect of temperature (indicated for each curve in K) on the current-density overpotential relationships for hydrogen evolution on illuminated p-GaP. Light intensity = 37 mW.cm^{-2}

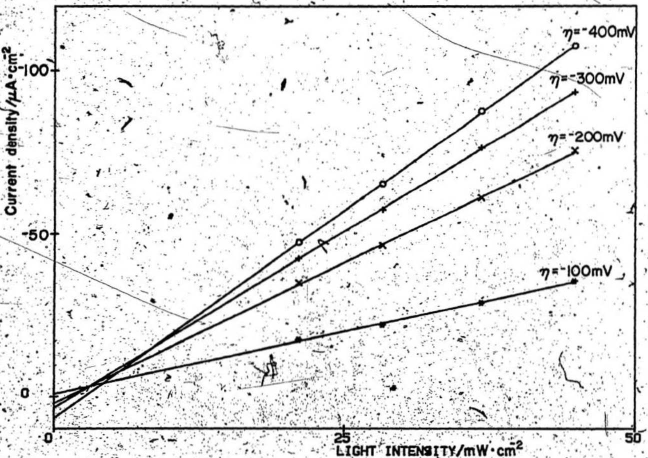

Figure 28: Representative current density vs. light intensity plots at several overpotentials (indicated at the end of each plot) for hydrogen evolution on p-GaP in 0.5 M H_2SO_4 at 306.8 K.

The good linearity exhibited by these plots was generally observed at each temperature and in all experiments. These plots were observed to very nearly intersect the origin, as expected. The deviations from zero current* at zero intensity are probably due to small errors in the light intensity values. The unavailability of data in the 0-20 mW.cm^{-2} range also tends to make the extrapolation less precise. It is, however, the slope of these plots that is required for the analysis, and, as mentioned above, the linearity over the intensity range studied is very good.

Ahlgren plots for several temperatures from one experiment with GaP are illustrated in Figure 29. Although there is appreciable scattering of the data about the least squares line of best fit, the intercepts at zero overpotential are significantly different for each temperature. The difference in these intercepts is also clear in Table 3, which summarizes results from two of the GaP experiments.

Table 3 also reveals a lack of reproducibility of the calculated exchange current densities at a particular temperature from one experiment to another. If the standard deviations of the values are considered, however, the exchange current densities overlap, or very nearly overlap, at all but one temperature. This is also apparent in Figure 30 which shows the Arrhenius plots for the two experiments. It is nevertheless clear from Figure 30 that the variation of the $\ln(i_{co})$

---

* The current would, strictly, not be zero at $I = o$ because of the finite dark current. The dark current is so small however that it cannot account for the deviations.

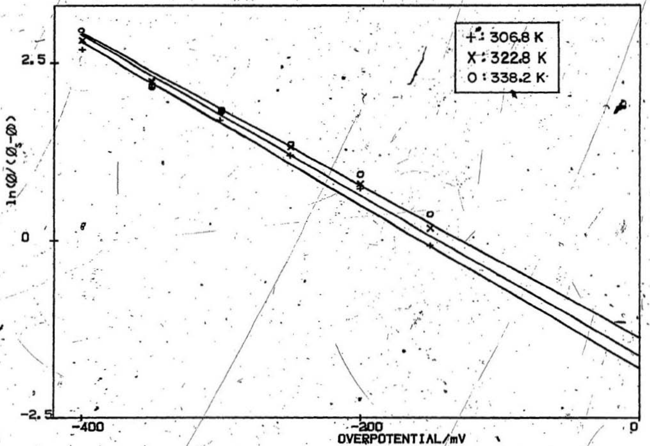

Figure 29. Typical Ahlgren plots at several temperatures for hydrogen evolution on illuminated p-GaP in 0.5 M H_2SO_4 (error bars omitted for clarity).

Table 3. Exchange current densities as a function of temperature for hydrogen evolution at illuminated p-GaP (two experiments).

(1) <u>Experiment T4</u>

Run	T/K	1000/T	ln(i_{co}/i_s)	i_s/μA.cm^{-2}	ln(i_{co}/μA.cm^{-2})
1*	322.7	3.099	-1.45(±0.17)	0.32	-2.58(±0.17)
2	275.9	3.625	-2.04(±0.22)	0.26	-3.39(±0.22)
3	291.5	3.431	-1.63(±0.15)	0.26	-2.98(±0.15)
4	307.2	3.255	-1.32(±0.18)	0.32	-2.46(±0.18)
5	338.8	2.952	-1.13(±0.23)	0.44	-1.95(±0.23)

(2) <u>Experiment T5</u>

Run	T/K	1000/T	ln(i_{co}/i_s)	i_s/μA.cm^{-2}	ln(i_{co}/μA.cm^{-2})
1	275.4	3.631	-2.35(±0.18)	0.26	-3.70(±0.18)
2	306.8	3.433	-1.81(±0.15)	0.29	-3.05(±0.15)
3	322.8	3.259	-1.63(±0.16)	0.31	-2.74(±0.16)
4	338.2	2.957	-1.38(±0.17)	0.37	-2.38(±0.17)

* This point omitted in the Arrhenius plot.

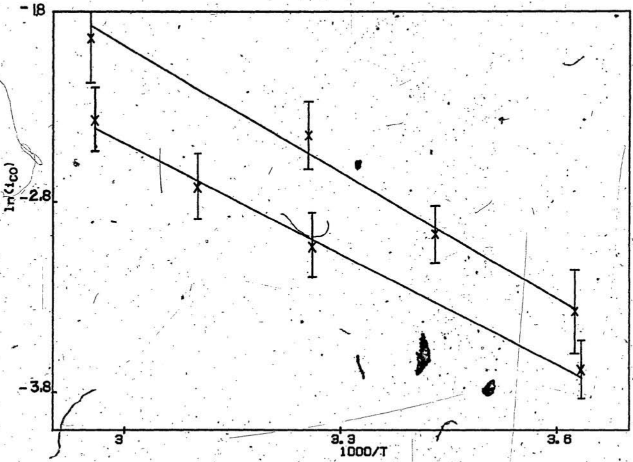

Figure 30. Arrhenius plots for hydrogen evolution on illuminated p-GaP in 0.5 M H_2SO_4 (from data of Table 3).

values at a particular temperature from one experiment to the next is quite systematic, with the entire Arrhenius plot being shifted by about the same amount. Thus the slope varies very little while the intercept (at 1000/T = 0) changes substantially from experiment to experiment.

The values of $\Delta H^{\ddagger}$ and $\ln(A^{\ddagger})$, obtained from weighted least squares analysis of the Arrhenius data, are given in Table 4 for the two experiments previously mentioned, and two additional experiments. There is some variation in the activation enthalpies obtained but the first three values agree rather well when the error limits are considered. Experiments T4, T5, and T6 were done, in order, using the same electrode, and a systematic trend is observed of decreasing $\Delta H^{\ddagger}$ and $A^{\ddagger}$ as the electrode ages. Quite considerable variation in the calculated pre-exponential factors is also observed. The weighted mean of the activation enthalpy, 16.0 kJ.mol^{-1}, is small in comparison to "usual" values obtained for electrochemical reactions. The above observations will be discussed further in Chapter V.

b. Gallium arsenide

Of the three semiconductors studied, GaAs gave the most problems of an experimental nature. Gallium arsenide electrodes were much more susceptible to problems of leakage and poor ohmic contact. They also survived for fewer experiments than the GaP and InP electrodes, i.e. sometimes leakage would occur soon (within a day or so) after the electrode was put into solution, before current-potential characteristics were reproducible or meaningful experiments had been started. Few GaAs electrodes endured for more than one experiment. Nevertheless, two reasonably successful variable temperature investigations were completed with GaAs.

Table 4. The values of $\Delta H^{\ddagger}$ and $\ln(A^{\ddagger})$ obtained from weighted least squares analysis of the Arrhenius plots for hydrogen evolution on illuminated p-GaP.

Experiment[1]	$\Delta H^{\ddagger}$/kJ.mol^{-1}	$\ln(A^{\ddagger}$/cm.s$^{-1})$
T3	16.3 ± 2.2	3.42 ± 0.94
T4	18.4 ± 1.7	4.65 ± 0.68
T5	16.0 ± 1.0	3.25 ± 0.38
T6	13.5 ± 1.[illegible]	2.29 ± 0.67
Weighted mean	16.0 ± 0.9	3.33 ± 0.41

[1] Experiments T4, T5 and T6 used the same electrode. A different electrode was used in T3.

The dependence of the current-potential curves for hydrogen evolution upon temperature (at constant light intensity) is illustrated in Figure 31. Figure 32 shows some current density vs. light intensity plots, at several overpotentials, for one temperature studied during one of the successful GaAs experiments. The plots were generally linear at all temperatures studied. Some of the Ahlgren plots at different temperatures, for the above experiment, are presented in Figure 33. Although there is noticeable deviation from linearity at both small and large overpotentials, the least squares-fitted lines and the intercepts at $\eta = 0$ are quite distinct for the three temperatures. A summary of the results for one of these experiments with GaAs is given in Table 5.

Arrhenius plots, constructed using data such as that of Table 5, for the two aforementioned "successful" experiments are illustrated in Figure 34. Only one of the plots exhibited good linearity and the actual values of $\ln(i_{co})$ at a given temperature again varied considerably from one experiment to the next. The slopes of the Arrhenius plots agreed reasonably well as is evident in the calculated $\Delta H^{\ddagger}$ values in Table 6. The weighted mean value of $\Delta H^{\ddagger}$, 25.7 kJ.mol^{-1}, is significantly larger than that found with GaP. The values of $\ln(A^{\ddagger})$, as Figure 34 suggests, are quite discordant. The above observations will be discussed further in the Discussion.

c. Indium phosphide

When the same experimental techniques as applied to GaP and GaAs were used to obtain data with InP, the initial results (the current-potential curves at different light intensities and the Ahlgren plots) suggested that the investigations were proceeding as expected based on

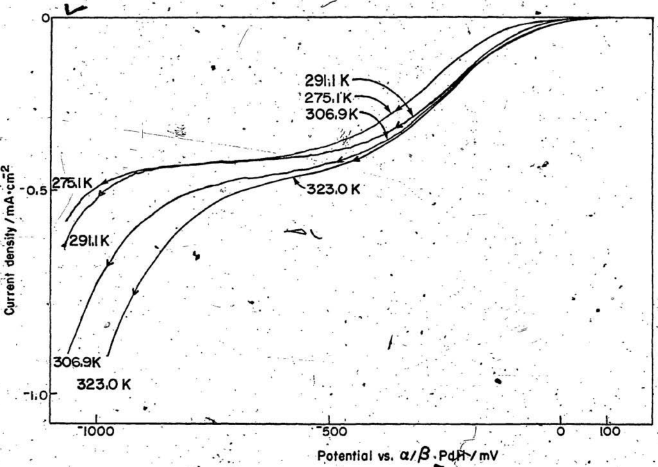

Figure 31: The temperature dependence of the current-potential curves for hydrogen evolution on p-GaAs in 0.5 M H_2SO_4. Light intensity = 21 mW.cm^{-2}. Temperatures given for each curve.

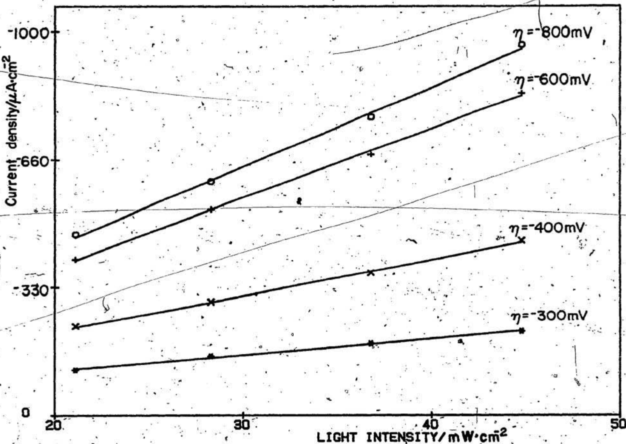

Figure 32. Typical current density vs. light intensity plots at several overpotentials (indicated at the end of each curve) for hydrogen evolution on p-GaAs in 0.5 M H_2SO_4. T = 306.9 K.

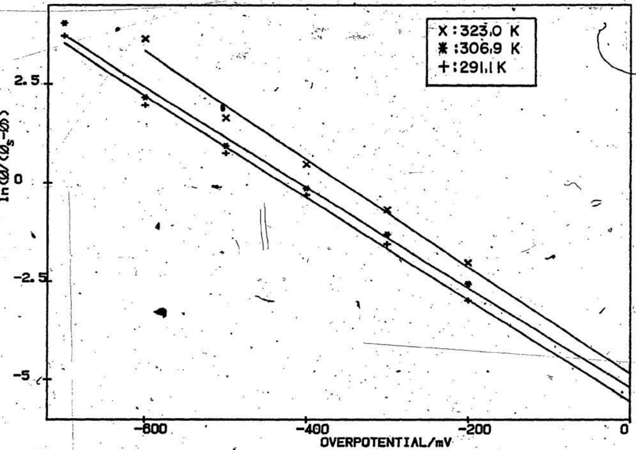

Figure 33. Representative Ahlgren plots at three temperatures for hydrogen evolution on illuminated p-GaAs in 0.5 M H_2SO_4.

Table 5. Exchange current densities as a function of temperature for hydrogen evolution at an illuminated p-GaAs electrode.

<u>Experiment T8</u>

Run	T/K	1000/T	$\ln(i_{co}/i_s)$	$i_s/\mu A.cm^{-2}$	$\ln(i_{co}/\mu A.cm^{-2})$
1	306.9	3.258	-5.20(±0.28)	11.2	-2.78(±0.28)
2	323.0	3.096	-4.85(±0.35)	14.7	-2.16(±0.35)
3	275.1	3.635	-5.14(±0.16)	3.5	-3.88(±0.16)
4	291.1	3.435	-5.54(±0.21)	9.2	-3.32(±0.21)

Table 6. The values of $\Delta H^{\ddagger}$ and $\ln(A^{\ddagger})$ obtained from weighted least squares analysis of the Arrhenius plots for hydrogen evolution on illuminated p-GaAs.

Experiment	$\Delta H^{\ddagger}/kJ.mol^{-1}$	$\ln(A^{\ddagger}/cm.s^{-1})$
T8	25.5(±1.4)	7.27(±0.50)
T19	29.9(±6.5)	8.04(±2.50)
weighted mean	25.7(±0.9)	7.30(±0.15)

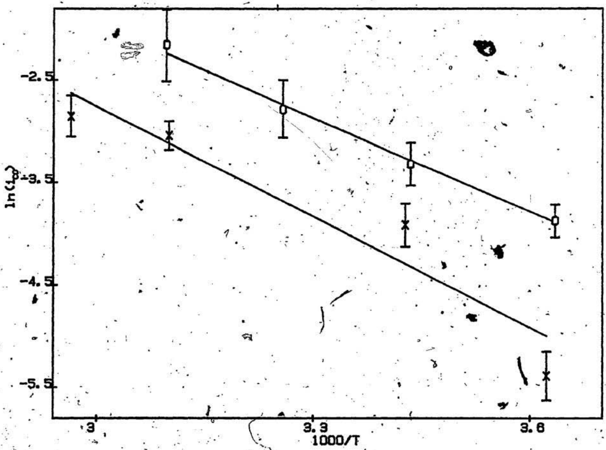

Figure 34. Arrhenius plots for hydrogen evolution on illuminated p-GaAs in 0.5 M H_2SO_4 (data from two experiments using different electrodes).

the GaP and GaAs results. The current-potential characteristics were reasonably reproducible and the Ahlgren plots were quite linear. It was soon discovered, however, that when the results from several temperatures were compared, the values of $\ln(i_{co})$, unlike those found in experiments using GaP and GaAs cathodes, exhibited considerable scatter (see Table 7).

Of particular note in Table 7 are the poor reproducibility of the results of the two experiments at ca. 307 K and the large discrepancies in the changes of $\ln(i_{co})$ for approximately equal changes in 1/T. It was subsequently learned that if a run at one temperature was repeated immediately, the current-potential characteristics were not reproducible. Instead there was a trend to increased current (at a given potential and light intensity) for the later run. If, however, a run was repeated after a "rest period" (electrode left at rest potential) of several hours, the current-potential curves displayed much better reproducibility.

It was therefore suspected that film formation was occurring on the InP during the cathodic potential sweep, a phenomenon reported previously (p. 61). Although visible films were not observed after the cathodic sweeps, it was suspected that an invisible film, if not removed before the next current-potential sweep, could sufficiently alter the condition of the InP surface so as to prevent reproducibility. For an electrode left for several hours at rest, the film dissolves and reproducible results are obtained. Film dissolution could be effected (see p. 63), by subjecting the InP electrode to a brief (30 s) anodic pulse at a potential some 100-200 mV positive of its rest potential, after every cathodic potential sweep. This anodic pulse treatment was

Table 7. Some results of early variable temperature work for hydrogen evolution on illuminated p-InP.

Run	T/K	1000/T	$\ln(i_{co}/i_s)$	$i_s/\mu A.cm^{-2}$	$\ln(i_{co}/\mu A.cm^{-2})$
1	275.9	3.625	-8.37 ± 0.15	1.4	-8.03 ± 0.15
2	291.4	3.432	-6.26 ± 0.24	1.7	-5.73 ± 0.24
7	291.5	3.431	-6.27 ± 0.21	1.7	-5.74 ± 0.21
3	307.1	3.256	-4.94 ± 0.20	2.5	-4.02 ± 0.20
6	306.7	3.261	-6.72 ± 0.21	2.5	-5.80 ± 0.21
4	322.9	3.097	-7.08 ± 0.19	4.2	-5.64 ± 0.19
5	337.2	2.966	-6.50 ± 0.18	5.8	-4.74 ± 0.18

employed in all subsequent experiments with InP, resulting in much more consistent behaviour.

Some of the results of these later experiments are summarized and illustrated in the following tables and figures. Current-potential curves at various temperatures (and constant light intensity) are shown in Figure 35. It was observed that a much more cathodic potential relative to the onset potential is required for InP relative to GaP before the current begins to increase rapidly (compare Figures 31 and 35). Otherwise the current-potential curves for InP and GaP are similiar.

Representative current density vs. light intensity plots at several overpotentials for one temperature are illustrated in Figure 36. Such excellent linearity was generally found for the later experiments with InP. Typical Ahlgren plots, from which the $\ln(i_{co})$ values at various temperatures were obtained, are shown in Figure 37. The good linearity, and distinct intercepts at $\eta = 0$ for different temperatures, were characteristic of the later experiments with InP. A summary of the results of one of these later experiments is presented in Table 8.

The results calculated from the Arrhenius plots for three of the later experiments using two different InP electrodes are given in Table 9. Two of the Arrhenius plots are shown in Figure 38. While the values of $\ln(i_{co})$ at a particular temperature do not agree very well, the figure demonstrates that the slopes of the two plots are in good agreement. This is reflected in Table 9 by the much greater relative variance in the $\ln(A^{\ddagger})$ values than in the $\Delta H^{\ddagger}$ values from the three experiments. The weighted mean $\Delta H^{\ddagger}$, 61.6 kJ.mol^{-1}, is considerably larger than that for the experiments using GaP and GaAs cathodes. Many of the above observations will be commented upon in the Discussion.

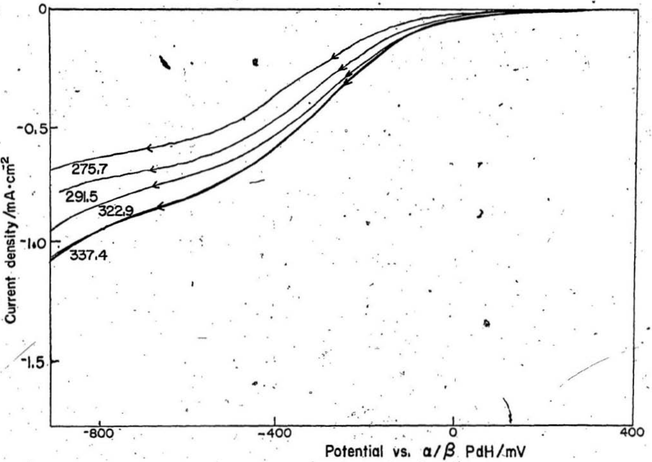

Figure 35. Current density-potential curves at various temperatures (indicated below each curve in K) for hydrogen evolution on p-InP in 0.5 M H_2SO_4. Light intensity = 21 mW.cm^{-2}.

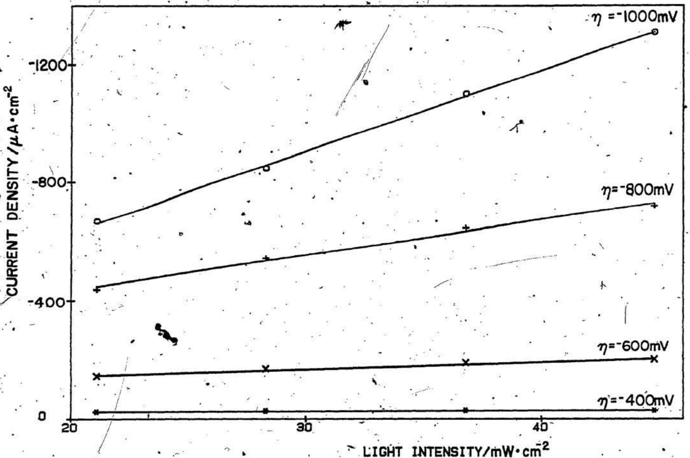

Figure 36. Typical current density vs. light intensity plots at several overpotentials (given above each plot) for hydrogen evolution on p-InP in 0.5 M H_2SO_4. T = 291.5 K.

Figure 37. Typical Ahlgren plots at several temperatures for hydrogen evolution on illuminated p-InP in 0.5 M H_2SO_4.

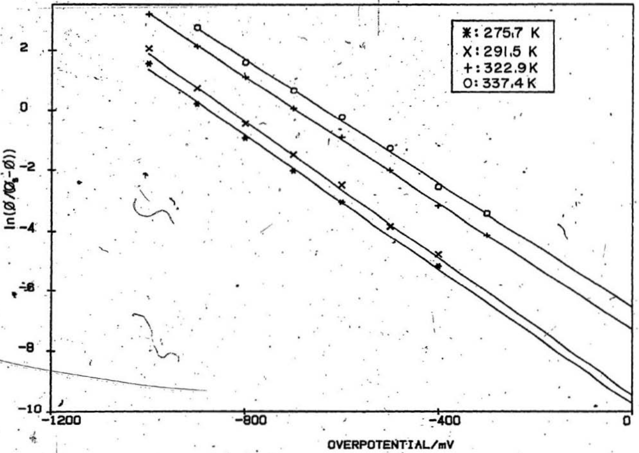
✱: 275.7 K
X: 291.5 K
+: 322.9 K
O: 337.4 K
2
0
-2
-4
-6
-8
-10
$\ln(\emptyset/(\emptyset_s-\emptyset))$
-1200
-800
-400
0
OVERPOTENTIAL/mV

Table 8. A summary of the results of one of the later variable temperature experiments with p-InP.

Experiment T16

Run	T/K	1000/T	$\ln(i_{co}/i_s)$	i_s/μA.cm^{-2}	$\ln(i_{co}$/μA.cm$^{-2})$
1	275.7	3.627	-9.72(±0.20)	1.4	-9.38(±0.20)
2	291.5	3.431	-9.42(±0.15)	1.7	-8.89(±0.15)
3	322.9	3.097	-7.29(±0.06)	4.2	-5.85(±0.06)
4	337.4	2.964	-6.54(±0.12)	5.8	-4.78(±0.12)

Table 9. A summary of the values of $\Delta H^{\ddagger}$ and $\ln(A^{\ddagger})$ for hydrogen evolution on illuminated p-InP obtained from the weighted least squares analysis of the Arrhenius plots for three different experiments.

Experiment[1]	$\Delta H^{\ddagger}$/kJ.mol^{-1}	$\ln(A^{\ddagger}$/cm.s$^{-1})$
T16	64.0 ± 7.0	17.9 ± 2.6
T18	59.1 ± 4.6	14.7 ± 1.8
T20	63.5 ± 5.4	16.4 ± 2.1
weighted mean	61.6 ± 1.6	16.0 ± 0.9

[1] Experiments T18 and T20 involved the same electrode. Experiment T16 employed a second specimen of InP.

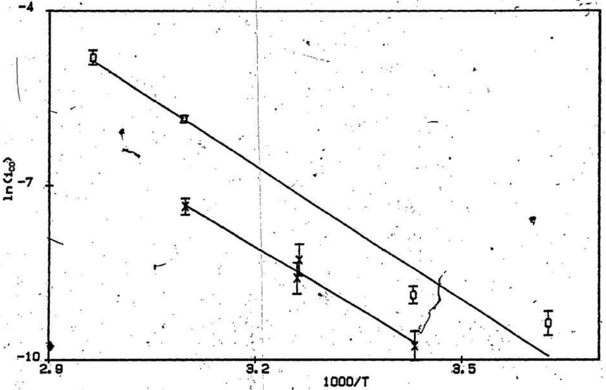

Figure 38. Arrhenius plots for hydrogen evolution on illuminated p-InP in 0.5 M H_2SO_4 (data from experiments using two different electrodes).

V. DISCUSSION

1. Noble Metal-Plating Experiments

As shown in the previous chapter, the presence of thin electrodeposits of platinum or palladium on the surface of GaP, GaAs and InP resulted in favourable (in the direction of positive potential) shifts of the current-potential characteristics for hydrogen evolution under illumination compared to those obtained in the absence of electrodeposits. Hence a smaller applied voltage is required for photo-assisted electrolysis on plated electrodes, resulting in slightly increased energy conversion efficiencies.

Plating is beneficial because it results in a semiconductor surface with sufficient quantities of the catalysts platinum or palladium to enhance the h.e.r. but not so much as to appreciably lower the light intensity reaching the semiconductor. The optimum metal coverage for current enhancement and long term stability was about 2 monolayers (for Pt and Pd, 1 atom.Å^{-2} ~ 5 monolayers) while coverages greater than about 500 monolayers resulted in metallic behavior of the electrode. The two monolayer coverage referred to above is almost certainly non-uniform, with alternating bare and plated areas, allowing the light to penetrate while providing many catalytic sites for completion of the h.e.r.

Although it was only on GaP that positive energy conversion efficiencies were realized, the favourable effect of noble metal-plating was also observed with InP and GaAs. Heller's group has recently had remarkable success by refining metal-plating techniques for p-InP (45,46). They used indium phosphide upon which catalyst islands of Pt or Rh had been created and a thin layer of oxide, presumably In_2O_3 or

$InPO_4$, formed. With this configuration they achieved 12% solar conversion efficiency for photo-assisted electrolysis in a Schottky-type cell producing H_2 and Cl_2 (45) and up to 11% efficiency for spontaneous photoelectrolysis (i.e. no bias voltage required) of HBr to H_2 and Br_2 using a p-InP cathode, treated as above, and an n-$MoSe_2$ anode (46). Their major achievement was the attainment of large current densities near the cathodic onset on p-InP as a result of the surface treatment, something which has not been accomplished by the methods employed in this work. Heller has not reported a problem of film formation during cathodic polarization of the surface-treated p-InP. Presumably, as found to a lesser degree in this research, the noble metal catalyst causes the h.e.r. to be the reaction preferred relative to film formation.

The idea of using a photoelectrolysis cell in which both anode and cathode are semiconductors was first suggested by Nozik (9). Such a configuration eases the restrictions on the positions of the semiconductor band edges relative to the H_3O^+/H_2 and O_2/H_2O redox couples and consequently on the onset potential for the desired reaction at each electrode (see Figure 39). If a photocathode with a more positive onset potential for H_2 evolution than the equilibrium potential (such as the plated GaP studied here or the modified InP referred to above) is combined with a photoanode with a more negative onset potential for O_2 evolution than that of a Pt anode, the conversion efficiencies become quite significant and spontaneous photoelectrolysis may even be possible, as demonstrated by Heller (45,46).

In summary, as techniques are developed to improve the current-potential characteristics and stability of semiconductor photoanodes

Figure 39. Hypothetical energy level diagrams for the spontaneous photoelectrolysis of water in a cell with 2 semiconductor electrodes with H_2 produced at the (p-type) cathode and O_2 produced at the (n-type) anode. Note that neither electrode could be used for spontaneous electrolysis if used in a Schottky-type cell with a metal counter electrode. Symbols: E_c - conduction band edge; E_v - valence band edge; E_F - Fermi level; $E_g(n)$, $E_g(p)$ - band gap energies of the n-type and p-type semiconductors, respectively. Based on a figure in (3).

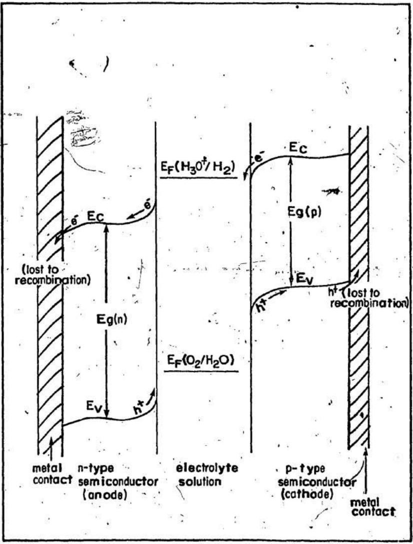
$E_F(H_3O^+/H_2)$
$E_F(O_2/H_2O)$
E_C
E_V
$E_g(n)$
$E_g(p)$
e^-
h^+
(lost to recombination)
metal contact
n-type semiconductor (anode)
electrolyte solution
p-type semiconductor (cathode)

and photocathodes, photoelectrolysis of water as a means of solar energy conversion may become more feasible.

2. Photoelectrochemical Kinetics Measurements

i. Agreement of results with theory

The current vs. light intensity plots without exception exhibited the anticipated linear behaviour and the individual Arrhenius plots also conformed well to the behaviour predicted. The data for Ahlgren plots, however, was often scattered quite noticeably about the least squares line of best fit and often showed slight curvature at both small and large overpotentials. This could be an indication that ρ, the fraction of the overpotential occurring in the Helmholtz layer, is somewhat dependent on the overpotential. It seems probable that at low and high overpotentials, where the current is beginning to flow or has saturated, respectively, ρ will vary somewhat from its value at intermediate overpotentials. At intermediate overpotentials, Ahlgren plots were reasonably linear and data in this range were usually emphasized in the construction of the plots.

The discussion of the slopes of the Ahlgren plots has been delayed until now. From equation [40], Chapter II, the slope is $-(1-\rho+\vec{\alpha}_c\rho)F/RT$. If $\rho = 0$, i.e. all of the overpotential occurs in the semiconductor space charge layer, the slope would be $-F/RT$ (ca. $-39V^{-1}$ at 298 K). If $\rho = 1$, i.e. all of the overpotential occurs in the Helmholtz layer of the electrolyte, the slope would be $-\vec{\alpha}_c F/RT$, enabling direct determination of the transfer coefficient, as suggested in Ahlgren's paper (20).

The difference in slope between experiments with different semiconductors was probably not significant, the average values at room temperature being 10.4, 12.0 and 11.6 V^{-1} for GaAs, GaP and InP, respectively, while no systematic variation in the slope with temperature was observed. The influence of temperature is unpredictable because the temperature dependence of ρ and α is unknown.

The slopes are much smaller than 39 V^{-1}, so the possibility of the overpotential occurring entirely in the semiconductor is excluded. Also, ρ must be greater than ca. 0.7 or else negative (physically unreasonable) values of $\vec{\alpha}_c$ would result. If ρ were unity, $\vec{\alpha}_c$ would be about 0.3, its maximum value according to the present observations. This suggests that the activated complex for the rate determining step of the h.e.r. on these semiconductors is decidedly reactant-like. It also implies that the overpotential occurring in the Helmholtz layer is quite significant, and may be dominant for hydrogen evolution on the semiconductors studied here, but it is not necessarily true that $\rho = 1$ as was assumed by Ahlgren (20).

ii. Difficulties encountered

The major disappointment was the poor reproducibility of the Arrhenius plots. As reported in Chapter IV, Arrhenius plots for individual experiments with a particular semiconductor cathode were generally reasonably linear. For different experiments, however, the exchange currents at each temperature were rarely in good agreement. The y-intercepts, i.e. the $\ln(A^{\ddagger})$ values from Arrhenius plots of data obtained with the same electrode material were very discordant, whereas the slopes (and hence $\Delta H^{\ddagger}$ values) demonstrated much better agreement.

For consecutive experiments with the same electrode, an increase in the true electrode area, caused by the roughening effects of etching and aging in solution, may partially account for the discrepancies mentioned, as the apparent area with an assumed roughness factor of unity was used for calculations. This area change on aging seems to be occurring in the consecutive experiments T4, T5 and T6, using the same GaP electrode (see Table 4, Results). An analytical method for the accurate determination of the true electrode area would be desirable.

The failure to achieve reproducible Arrhenius plots is without doubt linked to the difficulties of obtaining a stable surface condition. The semiconductors studied contained low concentrations of impurity donor atoms, so that their surface properties should be very sensitive to even small amounts of impurities in the electrolyte which become adsorbed on the surface. Difficulties in obtaining reproducible results are well known for electrochemical kinetic studies using metal electrodes, so it should be no surprise to encounter such problems when semiconductors, which may be expected to be more susceptible to impurities, are used as electrodes.

iii. The significance of the exchange current densities and enthalpies of activation determined here.

Recall from equation [40] of Chapter II that the exchange current density is determined from the intercept at $\eta = 0$ of a plot of $\ln(\phi/(\phi_s-\phi))$ vs. η. The values of the quantum yield and the quantum yield at saturation, ϕ and ϕ_s, respectively, are obtained from plots of current density (i) versus light intensity (I) at selected overpotentials. Since the quantum yields are independent of I a range of conveniently measurable light intensities was chosen (see Figure 28, for example).

In the dark, when equilibrium is established, the Fermi level of a semiconductor electrode is equal to that of the electrolyte solution with which it is in contact, here the equilibrium potential of the h.e.r. in 0.5 M H_2SO_4*. Upon illumination the Fermi level of the semiconductor changes, as the band bending is decreased, and a photopotential (or photovoltage) is measurable at open circuit. The magnitude of this photopotential, which determines the potential of zero current at the particular light intensity, is dependent on the light intensity (see Gerischer (47)).

As the light intensity is lowered, the potential of zero current in the light approaches the equilibrium potential in the dark and in the limit $I \to o$, the two potentials should be equal. The values of ϕ and ϕ_s are independent of the light intensity range used to find them, so that the Ahlgren plot, and hence the exchange current obtained from it, are also independent of the magnitude of the light intensities employed. The exchange currents determined by this method are then the same as those that would be obtained in the dark, at the equilibrium potential (which, as stated in the footnote, may be slightly different

---

* For true equilibrium of the h.e.r., appreciable quantities of both the reduced species, H_{ads} or H_2, and the oxidized species, H_3O^+, must be present. Thus 0.5 M H_2SO_4 with dissolved H_2 (i.e. under a constant pressure of H_2) is ideally required to meet this condition. However, as long as some dissolved H_2 or some H_{ads} is present, an equilibrium (rest) potential can be established which may be close to the equilibrium potential for the h.e.r. in 0.5 M H_2SO_4 at unit fugacity of H_2. In this work, it was observed that after a series of potential scans in the light producing H_2, the rest potential in the dark was near (within 50 mV at worst) this equilibrium potential.

from the equilibrium potential in 0.5 M H_2SO_4 at unit fugacity of H_2). The light intensity is simply the variable which enables one to determine the exchange current.

Ahlgren's approach (20), of using the equilibrium potential for the reaction being studied as his $\eta = 0$ for the plot of $\ln(\phi/(\phi_s-\phi))$ vs. η is now seen to have another flaw. Although the current density-light intensity plots do not depend on I, the potential of zero current does so depend while Ahlgren's potential for $\eta = 0$ remains constant. Therefore, the overpotential assigned to the i vs. I plots will vary with light intensity and hence the exchange current densities determined will decrease if smaller light intensities are used for the measurements, as illustrated in Figure 40.

With the above considerations, comparison of the exchange current densities for the h.e.r. on the different semiconductors studied here and on metal electrodes in the same (or similiar) electrolytes should be valid, at least at the order of magnitude level*.

The $\Delta H^{\ddagger}$ values are determined from Arrhenius plots of the exchange current densities at different temperatures. They thus refer to a potential, on each semiconductor, for which the potential energy barrier is the same from the reactants' or products' side (and thus ΔH for the reaction is zero), in agreement with Randles' definition (48), and should be comparable from semiconductor to semiconductor.

iv. Exchange currents

The exchange current densities at room temperature for the h.e.r. on the semiconductor electrodes studied here (interpolated from the

---

* Since, as discussed previously, the equilibrium potentials for the h.e.r. may vary a little on the semiconductor electrodes.

Figure 40. Hypothetical Ahlgren plots showing the effect of the relative magnitude of the light intensities used upon the values of the exchange current density obtained when 2 different conventions for $\eta = 0$ are followed. The intercept varies with Ahlgren's convention (20) because the potential of zero current shifts with light intensity so the overpotential to which particular current density-light intensity plots (from which the values of ϕ are obtained) refer is not invariant.

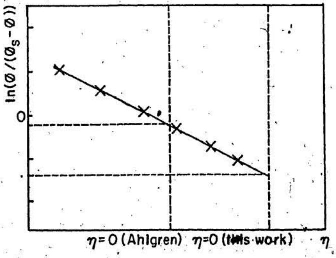

(a) from measurements at relatively high light intensities.

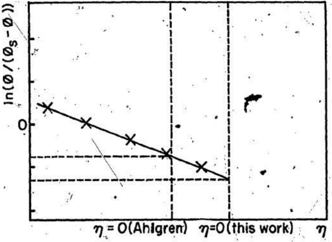

(b) from measurements at relatively low light intensities.

Arrhenius plots), and on several metals, are given in Table 10. GaP, GaAs and InP are intermediate in catalytic activity for the h.e.r., being less effective than such well-known excellent catalysts as Pd and Pt but better than such poor catalysts as Ga, In, Pb and Hg.

InP may be poorer than GaP and GaAs as an h.e.r. electrode because of the cathodic film which forms on it in competition with the h.e.r. and perhaps partially because In is a poorer h.e.r. catalyst than Ga.

v. Activation enthalpies

A comparison of the activation enthalpies and pre-exponential factors for the h.e.r. on the three semiconductors of this thesis (Table 11) shows that the activation barrier for the h.e.r. is greatest on InP, significantly smaller on GaAs and smaller still on GaP. The values of $\ln(A^{\ddagger})$ show the opposite trend. These results apply to the bare electrode surfaces, and as was seen here and in Heller's results (45,46), plating of thin noble metal films and other surface treatments may greatly facilitate the h.e.r.

vi. Summary - future research

In view of Heller's dramatic successes it would be instructive to extend his specific surface treatments to GaP and GaAs and to use the methods of this thesis to investigate the effect of such treatments on the kinetics of the h.e.r. at these electrodes. Specifically, one might expect to find a decrease in $\Delta H^{\ddagger}$ or an increase in $A^{\ddagger}$ or both and an increase in exchange current density following these treatments.

In summary, the results of this thesis agreed reasonably well with the theory so far developed, enabling the calculation of kinetic parameters for the h.e.r. on the three semiconductors studied. Such data can be used in conjunction with thermodynamic results to predict the feasibility of use of these materials in solar energy conversion.

Table 10. Exchange current densities on some metals[1] and on the semiconductor electrodes studied here for the h.e.r. at 298 K.

Electrode material	$\log_{10}(i_{co}/\mu$[illegible]$cm^{-2})$
Pt	4.3
Pd	4.0
Ti	-1.0
GaP	-1.3
GaAs	-1.5
InP	-3.7
Ga	-4.0
In	-5.0
Tl	[illegible]5.0
Pb	-5.5
Hg	-6.0

[1] Calculated from data of Krishtalik (25) for acid solutions.

Table 11. Comparison of the activation enthalpies and pre-exponential factors calculated from the Arrhenius plots for the h.e.r. on the three semiconductors studied in this work.

Semiconductor cathode	$\Delta H^{\ddagger}/kJ.mol^{-1}$	$\ln(A^{\ddagger}/cm.s^{-1})$
GaP	16.0 ± 0.9	3.3 ± 0.4
GaAs	25.7 ± 0.9	7.3 ± 0.2
InP	61.6 ± 1.6	16.0 ± 0.9

REFERENCES

1. A. Fujishima and K. Honda, Nature, 1972, 238, 37.

2. L.A. Harris and R.H. Wilson, Ann. Rev. Mater. Sci., 1978, 8, 99.

3. A.J. Nozik, Ann. Rev. Phys. Chem., 1978, 29, 189.

4. M. Tomkiewicz and H. Fay, Appl. Phys., 1979, 18, 1.

5. B. Parkinson, J. Chem. Ed., 1983, 60, 338.

6. R. Memming and G. Schwandt, J. Electrochem. Soc., 1969, 116, 785.

7. J. O'M. Bockris and K. Uosaki, J. Electrochem. Soc., 1977, 124, 98.

8a. M. Tomkiewicz and J. Woodall, Science, 1977, 196, 991.

8b. M. Tomkiewicz and J. Woodall, J. Electrochem. Soc., 1977, 124, 1436.

9. A.J. Nozik, Appl. Phys. Lett., 1976, 29, 150.

10. K. Ohashi et al., Nature, 1977, 266, 610.

11. H. Tamura et al., J. Electroanal. Chem., 1977, 80, 357.

12. M.P. Dare-Edwards et al., J. Electroanal. Chem., 1981, 119, 109.

13a. M.A. Butler and D.S. Ginley, J. Electrochem. Soc., 1980, 127, 1273.

13b. M.A. Butler and D.S. Ginley, Appl. Phys. Lett., 1983, 42, 582.

14. A. Bourasse and G. Horowitz, J. Phys. Lett., 1977, 38, L-291.

15. K. Uosaki and H. Kita, J. Electrochem. Soc., 1981, 128, 2153.

16. F.R. Fan and A.J. Bard, J. Am. Chem. Soc., 1980, 102, 3677.

17. Y. Nakato et al., Ber. Bunsenges. Phys. Chem., 1976, 80, 1289.

18. M.S. Wrighton, J. Chem. Ed., 1983, 60, 335.

19. A.B. Bocarsly et al., J. Am. Chem. Soc., 1980, 102, 3683.

20. W.L. Ahlgren, J. Electrochem. Soc., 1981, 128, 2123.

21. W.L. Ahlgren, M.S. Thesis, The University of Arizona, Tuscon, 1977.

22. J.F. Dewald in Semiconductors, N.B. Hannay, editor, Reinhold, New York, 1959, p. 727.

23a. H. Gerischer in Physical Chemistry: An Advanced Treatise, Vol. IXA, H. Eyring, D. Henderson, W. Jost, editors, Academic Press, New York, 1970, p. 472.

23b. H. Gerischer in Advances in Electrochemistry and Electrochemical Engineering, Vol. 1, P. Delahay and C. Tobias, editors, Interscience, New York, 1961, p. 139.

24. H. Gerischer et al., J. Electroanal. Chem., 1981, 119, 41.

25. L.I. Krishtalik in Advances in Electrochemistry and Electrochemical Engineering, Vol. 7, P. Delahay, editor, Interscience, New York, 1970, p. 283.

26. W.H. Brattain and C.G.B. Garrett, Bell Syst. Tech. J., 1955, 34, 129.

27. V.A. Myamlin and Y.V. Pleskov, The Electrochemistry of Semiconductors, Plenum, New York, 1967.

28. M. Green in Modern Aspects of Electrochemistry, Vol. 2, J. Bockris, editor, Butterworths, London, 1959, p. 343.

29. A. Bocarsly et al., J. Am. Chem. Soc., 1980, 102, 3683.

30. R. Dominey et al., J. Am. Chem. Soc., 1981, 103, 1261.

31. W.W. Gartner, Phys. Rev., 1959, 116, 84.

32. R.H. Wilson, J. Appl. Phys., 1977, 48, 4292.

33. G. Horowitz, Appl. Phys. Lett., 1982, 40, 409.

34. W. Lorenz and S. Handschuh, Physica Status Solidi:A, 1982, 71, 127.

35. K. Ohashi et al., Energy Research, 1977, 1, 25.

36. K. Uosaki, Ph.D. Thesis, The Flinders University of South Australia, Adelaide, 1977.

37. P. Kohl and A.J. Bard, J. Am. Chem. Soc., 1977, 99, 7531.

38. G. Hills and D. Ives in Reference Electrodes, D. Ives and G. Janz, editors, Academic Press, New York, 1961, p. 71.

39. F. Lewis, The Palladium/Hydrogen System, Academic Press, London, 1967.

40. P.J. Holmes in The Electrochemistry of Semiconductors, P.J. Holmes, editor, Academic Press, London, 1962, p. 372.

41. A. Heller et al., J. Am. Chem. Soc., 1980, 102, 6555.

42. W. Albery and P. Bartlett, J. Electrochem. Soc., 1982, 129, 2254.

43. S. Mayumi et al., Denki Kagaku, 1976, 44, 5.

44. K. Uosaki and H. Kita, Solar Energy Mater., 1983, 7, 421.

45. A. Heller and R. Vadimsky, Phys. Rev. Lett., 1981, 46, 1153.

46. C. Levy-Clement et al., J. Electrochem. Soc., 1982, 129, 1701.

47. H. Gerischer, Electroanal. Chem. and Interfac. Electrochem., 1975, 58, 263.

48. J.E.B. Randles, Trans. Faraday Soc., 1952, 48, 828.

APPENDIX

The detailed solution of equation [27], p. 20, and subsequent development to arrive at equation [32], p. 21, is given below.

At a distance x into the semiconductor, the time rate of change of the electron concentration, $\frac{dn(x)}{dt}$, is given by

$$\frac{dn(x)}{dt} = g(x) + d(x) - r(x) \qquad [A1]$$

where g(x) is the rate of electron generation due to light absorption, r(x) is the electron-hole recombination rate, and d(x) is the rate of change of n(x) due to diffusion.

Using the quasi-equilibrium (steady-state) assumption (i.e. $\frac{dn(x)}{dt} = 0$) gives:

$$d(x) = -g(x) + r(x) \qquad [A2]$$

From equations [26], [24], and [27] of Chapter II, one can write

$$d(x) = H\left(\frac{d^2n(x)}{dx^2}\right) \text{ where } H = D_n = \frac{L_n^2}{\tau_n} \qquad [A3]$$

$$g(x) = G \exp(-\bar{a}x) \quad \text{where } G = \frac{\bar{a}\gamma I}{e} \qquad [A4]$$

$$r(x) = \frac{n(x)-n_o}{\tau_n} \qquad [A5]$$

so that [A2] now becomes,

$$\frac{d^2 n(x)}{dx^2} - \frac{n(x)}{H\tau_n} = \frac{-G}{H} \exp(-\bar{a}x) - \frac{n_o}{H\tau_n} \qquad [A6]$$

The inhomogeneous differential equation [A6] may be solved by the method of undetermined coefficients, i.e.

$$n(x) = n_h(x) + n_i(x) \qquad [A7]$$

where $n_h(x)$ and $n_i(x)$ are solutions to the homogeneous and inhomogeneous parts of [A6], respectively. Thus,

$$n_h(x) = C_1 \exp(\frac{x}{L_n}) + C_2 \exp(\frac{-x}{L_n}) \qquad [A8]$$

where C_1 and C_2 are to be determined, and

$$n_i(x) = A \exp(-\bar{a}x) + B \qquad [A9]$$

where A and B are constants to be determined by substituting $n_i(x)$ and $\frac{d^2 n_i(x)}{dx^2}$ found from [A9] into [A6]. The result is

$$n_i(x) = \frac{G}{\left\{\frac{1}{\tau_n} - (\bar{a})^2 H\right\}} \exp(-\bar{a}x) + n_o \qquad [A10]$$

The solution of [A6] is then:

$$n(x) = C_1 \exp(\frac{x}{L_n}) + C_2 \exp(\frac{-x}{L_n}) + \frac{G}{\left\{\frac{1}{\tau_n} - (\bar{a})^2 H\right\}} \exp(-\bar{a}x) + n_o \qquad [A11]$$

By imposing the boundary conditions of the problem,

$$n \rightarrow n_o \text{ as } x \rightarrow \infty$$

$$n = n_w \text{ at } x = w \qquad [A12]$$

the constants C_1 and C_2 may be evaluated and the complete solution of [A6] becomes

$$n(x) = \left[n_w - n_o - \frac{G}{\left\{ \frac{1}{\tau_n} - (\bar{a})^2 H \right\}} \exp(-\bar{a}x) \right] \exp\left(\frac{w}{L_n}\right) \exp\left(\frac{-x}{L_n}\right) + \left[\frac{G}{\left\{ \frac{1}{\tau_n} - (\bar{a})^2 H \right\}} \exp(-\bar{a}x) \right] + n_o \qquad [A13]$$

To evaluate $\vec{J}_n$, the electron flux entering the depletion layer from the bulk, by diffusion, one first rewrites [25],

$$J_n = \frac{-L_n^2}{\tau_n} \left(\frac{dn}{dx}\right)_{x=w} \qquad [A14]$$

which is written for flux in the positive x-direction. $\vec{J}_n$, however, is, particularly, in the negative x-direction so

$$\vec{J}_n = \frac{L_n^2}{\tau_n} \left(\frac{dn}{dx}\right)_{x=w} \qquad [A15]$$

Equation [A13] is used directly to evaluate $\frac{dn}{dx}$, w is substituted for x to give $\left(\frac{dn}{dx}\right)_{x=w}$ and the result used in [A15] to yield

$$\vec{J}_n = \frac{-L_n}{\tau_n}(n_w - n_o) + \frac{\bar{a}L_n\gamma I(\exp(-\bar{a}w))}{e(1 + \bar{a}L_n)} \qquad [A16]$$

where substitutions for G and H have been made using [A3] and [A4]. Equation [A16] is the same as equation [30] of Chapter II.

The minority carrier balance over the entire depletion layer, [A17], (equation [31] of Chapter II),

$$\int_0^w g(x)\,dx - \nu_s(n_w - n_o) = \frac{-i_c}{e} - \vec{J}_n \qquad [A17]$$

can be evaluated using [A16] and [A4] to give

$$\frac{\gamma I}{e}(1-\exp(-\bar{a}w)) - \nu_s(n_w - n_o) = \frac{-i_c}{e} + \frac{L_n}{\tau_n}(n_w - n_o) - \frac{\bar{a}L_n\gamma I(\exp(-\bar{a}w))}{e(1 + \bar{a}L_n)} \qquad [A18]$$

By collecting the $(n_w - n_o)$ terms, [A18] can be simplified to

$$\frac{n_w}{n_o} = \frac{i_c + \gamma I\left[1 - \frac{\exp(-\bar{a}w)}{(1 + \bar{a}L_n)}\right]}{en_o\left\{\nu_s + \frac{L_n}{\tau_n}\right\}} + 1 \qquad [A19]$$

which is equation [32] of Chapter II.